nature communications

Article

https://doi.org/10.1038/s41467-024-55389-2

Excitable Ras dynamics-based screens reveal RasGEFX is required for macropinocytosis and random cell migration

Received: 1 October 2023

Accepted: 8 December 2024

Published online: 02 January 2025

Check for updates

Koji Iwamoto [1], Satomi Matsuoka [1,2,3] ✉ & Masahiro Ueda [1,2] ✉

Excitable systems of eukaryotic chemotaxis can generate asymmetric signals of Ras-GTP-enriched domains spontaneously to drive random cell migration without guidance cues. However, the molecules responsible for the spontaneous signal generation remain elusive. Here, we characterized RasGEFs encoded in *Dictyostelium discoideum* by live-cell imaging of the spatiotemporal dynamics of Ras-GTP and hierarchical clustering, finding that RasGEFX is primarily required for the spontaneous generation of Ras-GTP-enriched domains and is essential for random migration in combination with RasGEFB/M/U in starved cells, and they are dispensable for chemotaxis to chemoattractant cAMP. RasGEFX and RasGEFB that co-localize with Ras-GTP regulate the temporal periods and spatial sizes of the oscillatory Ras-GTP waves propagating along the membrane, respectively, and thus control the protrusions of motile cells differently, while RasGEFU and RasGEFM regulate adhesion and migration speed, respectively. Remarkably, RasGEFX is also important for Ras/PIP3-driven macropinocytosis in proliferating cells, but RasGEFB/M/U are not. These findings illustrate a specific and coordinated control of the cytoskeletal dynamics by multiple RasGEFs for spontaneous motility and macropinocytosis.

Spontaneous activity is one of the hallmarks of living organisms. Spontaneous cell migration is a typical example of spontaneous activity and describes how various cells exhibit motile function in a random manner without environmental guidance cues, which is a basis for directed cell migration[1–6]. Recent studies have demonstrated that excitable systems of chemotaxis generate an asymmetric signal to regulate cell motility spontaneously by breaking symmetry in the intracellular distribution of various signaling molecules, including Ras, PI3K, PI(3,4,5)P3, Akt/PKB and Scar/WAVE at the "front" region of motile cells and PTEN, PI(4,5)P2 and CynA at the "back" region[7–12]. Such excitable systems are conserved evolutionarily in the chemotactic signaling networks of various cell types from the lower eukaryote *Dictyostelium discoideum* to human leukocytes[11,13–17]. However, our understanding of how spontaneous dynamics emerge from excitable systems is limited because the molecules that trigger symmetry breaking have not been identified.

Ras family small GTPases are key molecules for the regulation of cellular anterior-posterior polarity and motility in various motile cells as well as macropinocytosis and phagocytosis in proliferating cells[11,18–21]. In *Dictyostelium* cells, there are multiple signaling pathways (RasG/PI3K, RasC/TorC2, Rap1/sGC, PLA2 and ErkB pathways) operating in parallel for chemotaxis, in which the small GTPases Ras/Rap proteins work as upstream regulators. The active form of Ras, Ras-GTP, can generate a Ras-GTP-enriched signaling domain on the plasma membrane to regulate cytoskeletal dynamics at the front region of motile cells during early starvation after axenic culture[4,8,22,23]. This signaling domain exhibits stereotypical characteristics of an excitable system, including spontaneous excitation, stimulation-induced

[1]Laboratory of Single Molecule Biology, Graduate School of Science and Graduate School of Frontier Biosciences, Osaka University, 1-3 Yamadaoka, Suita, Osaka 565-0871, Japan. [2]Laboratory for Cell Signaling Dynamics, Center for Biosystems Dynamics Research (BDR), RIKEN, 1-3 Yamadaoka, Suita, Osaka 565-0871, Japan. [3]PRESTO, JST, 1-3 Yamadaoka, Suita, Osaka 565-0871, Japan. ✉e-mail: ueda.masahiro.fbs@osaka-u.ac.jp; matsuoka.satomi.fbs@osaka-u.ac.jp

excitation and traveling wave generation[11,14,15,24–28]. For example, the Ras-GTP-enriched domain is generated transiently on the membrane in an all-or-none manner through spontaneous excitatory dynamics without the extracellular chemoattractant cAMP. Under enhanced excitability, the domain can exhibit traveling waves propagating continuously over the membrane as oscillatory dynamics[28,29]. The transition from excitatory to oscillatory dynamics can be manipulated experimentally by enhancing excitability with caffeine in *Dictyostelium* cells[28,30–32]. Further evidence for excitability includes chemoattractant-induced all-or-none excitation, in which the Ras-GTP-enriched domain is induced by a uniform stimulation of cAMP or biased spatially under cAMP gradients toward the higher concentration side[27,33,34]. The spontaneous generation of the Ras-GTP-enriched domain does not require signaling molecules downstream of Ras/Rap in the four major signaling pathways including PI3K, PTEN, PI(3,4,5)P3, TorC2, sGC and PLA2[28,33–36], meaning that the Ras-GTP-enriched domain can be generated without the intrinsic activities of downstream pathways under no chemoattractant. Thus, identifying the molecules responsible for the Ras excitability is key to understanding the spontaneous symmetry breaking for cell motility.

Ras activity is regulated by guanine nucleotide exchange factors (RasGEFs) and GTPase-activating proteins (RasGAPs)[37,38]. So far, 25 genes for RasGEFs have been found in the *Dictyostelium discoideum* genome, with several RasGEFs considered potential regulators of Ras[39–44]. Upon cAMP binding to the receptor cAR1, chemotaxis signaling via the heterotrimeric G protein $G\alpha_2\beta\gamma$ leads to the activation of Ras, in which RasGEFA and RasGEFH activate RasC, and RasGEFR and RasGEFF activate RasG[41,43,44]. Additionally, RasGEFQ and RasGEFU activate RasB and Rap1 upon cAMP stimulation, respectively[40,42]. However, the contributions of these and other RasGEFs to the spontaneous dynamics of excitable systems are unknown, because a systematic and comprehensive analysis of RasGEFs on Ras excitability without chemoattractants has never been performed.

Ras GTPases have been also identified as a key regulator for macropinocytosis. Macropinocytosis is an evolutionarily conserved fluid-phase endocytosis, by which extracellular fluid is nonselectively uptaken into cells, providing diverse functions in a variety of cell types[45]. In mammals, macropinocytosis is critical for nutrient acquisition and immune response[46]. Cancer cells exploit macropinocytosis to sustain cell proliferation by absorbing extracellular proteins and fatty acids under nutrient-limited conditions, and macropinocytosis can be induced by oncogenic Ras[47,48]. In *Dictyostelium discoideum*, macropinocytosis facilitates the uptake of nutrients in the growth stage[49]. Recent studies using *Dictyostelium* cells have revealed various signaling molecules including Ras, PI3K, PI(3,4,5)P3 and RasGAPs such as IqgC, some of which are common for chemotaxis. These molecules accumulate at the macropinocytic cup, driving macropinocytosis through the remodeling of the actin cytoskeleton[21,50–52]. However, RasGEFs that regulate Ras activity for macropinocytosis have not been identified in *Dictyostelium* cells or other cell types.

In this study, we developed a screening method to identify the RasGEFs responsible for the spontaneous generation of Ras-GTP-enriched domains in random cell migration. We utilized starved *D. discoideum* cells for the screening because they can exhibit enhanced amoeboid movement with actin cytoskeleton-dependent protrusions more obviously than vegetative cells, which are remarkable for macropinocytosis[11,21,50,53–58]. We identified a specific RasGEF as an essential component of the pathway that triggers symmetry breaking in the excitable system to generate internal Ras-GTP-enriched signals. RasGEFX is primarily required for the asymmetric generation of Ras-GTP signals and is essential for random cell migration with RasGEFB/M/U in starved cells. Notably, RasGEFX is also important for macropinocytosis in vegetative cells at the growth stage, but RasGEFB/M/U are not. From these observations, we propose that multiple RasGEFs constitute a spontaneous and excitable signal generator to drive random cell motility and some contribute to Ras regulation in macropinocytosis.

Results

Comprehensive characterization of RasGEFs in Ras excitability

RBD_{Raf1} is a commonly used probe of Ras-GTP in the signaling domain generated at the front of motile cells during early starvation after axenic culture[22,33,59]. Biochemical evidence has revealed that RBD_{Raf1} can bind at least to RasG and RasC in vitro[22,60,61]. To reveal which Ras molecules are detected with this probe among those of the multiple parallel signaling pathways in living cells, we analyzed the membrane localization of fluorescently labeled RBD_{Raf1} in single, double and triple knockout strains (SKO, DKO, and TKO, respectively) of RasG, RasC and Rap1. When fluorescently labeled RBD_{Raf1} was observed in cells treated with 10 μM latrunculin A, an inhibitor of actin polymerization, and also with 4 mM caffeine, which can enhance Ras excitability[14,28,31], the fraction of cells showing membrane localization of RBD_{Raf1} was significantly reduced in the *rasG-/rapA-* DKO strain, although RBD_{Raf1} was obviously localized on the membrane in all SKO and other DKO strains (Fig. 1a, b and Supplementary Table 1), showing that RBD_{Raf1} can localize to the membrane normally when either RasG or Rap1 is expressed. Further reduction was observed in the *rasG-/rasC-/rapA-* TKO strain, showing the involvement of RasC in the membrane localization of RBD_{Raf1}. Without caffeine, the Ras-GTP probe exhibited almost no membrane localization in *rasG-/rasC-/rapA-* cells, showing that these three small GTPase are the primary factors in the membrane localization of RBD_{Raf1} (Supplementary Fig. 1a, b and Supplementary Table 1). Moreover, a small fraction of cells still exhibited membrane localization when treated with caffeine, indicating that RBD_{Raf1} can detect the activities of other Ras proteins when excitability is enhanced by caffeine. Fluorescence tagging, which was prepared with RFP, mScarlet-I or GFP, did not affect significantly the probe function (Supplementary Fig. 1c, d and Supplementary Table 2). These observations indicate that a mixture of Ras molecules is activated in the Ras-GTP-enriched domain. In the following experiments, we utilized RBD_{Raf1} as a probe to observe the mixed activity of Ras/Rap1.

To identify the RasGEFs responsible for spontaneous Ras excitation, we characterized the spatiotemporal dynamics of the Ras-GTP-enriched domain when RasGEFs were overexpressed. We prepared a series of cell strains overexpressing (OE) one of 25 RasGEFs tagged to GFP and co-expressed them with RBD_{Raf1}-RFP[22,61] (Fig. 1c, d). Three transformants (RasGEFI/J/Q) were unstable for the expression of RBD_{Raf1}-RFP and thus excluded from the subsequent analysis. To compare the effects of each OE strain on the spatiotemporal dynamics of Ras-GTP, the cells were treated with 10 μM latrunculin A to exclude the effects of the cell shape on the Ras-GTP distribution and treated with 4 mM caffeine to induce the oscillatory dynamics (Supplementary Movie 1). Under these conditions, the spatiotemporal dynamics that can be observed in wild-type (WT) cells showed four patterns: no generation of the Ras-GTP-enriched domain (no domain), transient generation of the domain (transient), traveling waves (wave) and uniform localization along the whole membrane (uniform), with increasing excitability in this order[28,30] (Fig. 1e and Supplementary Movie 1). These four patterns exhibited cell-to-cell heterogeneity in Ras dynamics, probably due to the balance between RasGEFs and RasGAPs expressed endogenously in a WT cell. The exogenous expression of each RasGEF modulated the balance differently. In cells of normal size, a single domain was usually observed in the transient and wave patterns.

The four patterns were distinguished by kymographs of the RBD_{Raf1}-RFP intensity measured along the cell periphery and by a hierarchical clustering analysis[62] (Supplementary Fig. 2a–f). The fractions of the patterns in WT cells were 25.5 ± 5.4% (no domain), 13.8 ± 6.3% (transient), 57.2 ± 2.5% (wave) and 3.4 ± 1.7% (uniform)

https://doi.org/10.1038/s41467-024-55389-2

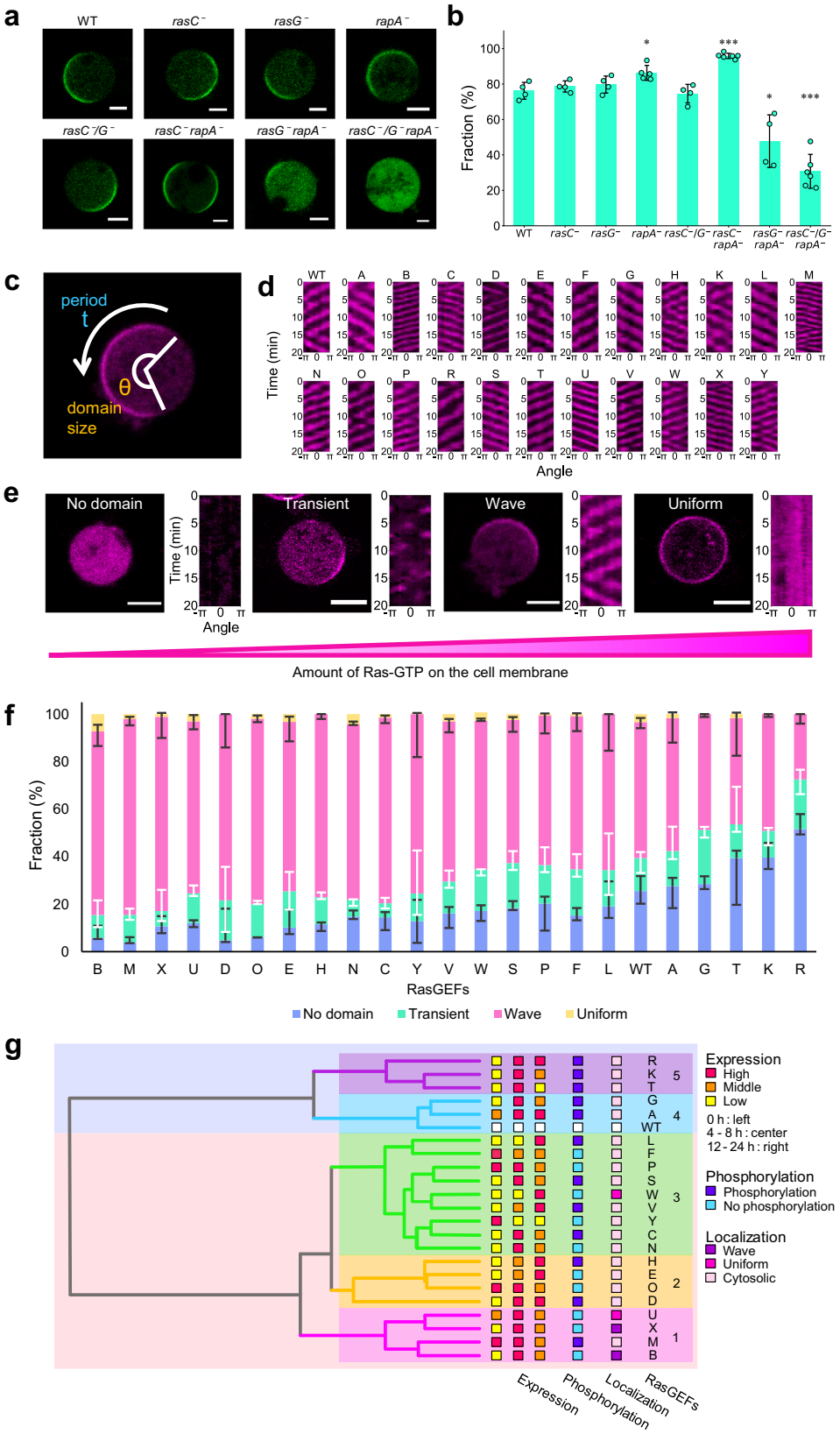

(Fig. 1f and Supplementary Tables 3, 4). The domain size and the oscillation period of the traveling waves in WT cells were 139.1 ± 61.0° and 244.0 ± 81.8 s, respectively (Supplementary Fig. 2g, h and Supplementary Tables 3, 4). As shown in the subsequent analysis, these characteristics of the spatiotemporal dynamics of the Ras-GTP-enriched domain differed depending on the type of RasGEF overexpressed, allowing us to screen for the RasGEFs responsible for spontaneous Ras excitation.

We found that the overexpression of a RasGEF acts either positively or negatively on Ras excitability. When compared with WT cells, the fraction of cells showing traveling waves was increased in the majority of RasGEF OE strains (B/M/X/U/D/O/E/H/N/C/Y/V/W/S/P/F/L)

Fig. 1 | Screening of RasGEFs essential for spontaneous Ras excitability. a, b RBD_{Raf1} localization in WT and Ras KO strains in the presence of caffeine. Cells were starved for 3 h. **a** Representative images of cells expressing RBD_{Raf1}-GFP from 3 independent experiments. Scale bars, 5 μm. **b** Fraction of cells showing RBD_{Raf1} membrane localization. Data are presented as the mean ± SD. n = 214, 176, 216, 92, 223, 315, 336 and 161 cells from 4, 4, 4, 5, 4, 6, 4 and 6 independent experiments for WT, *rasC-*, *rasG-*, *rapA-*, *rasC-/G-*, *rasC- rapA-*, *rasG- rapA-* and *rasC-/G- rapA-*, respectively. * $p < 0.05$, *** $p < 0.001$; two-sided Welch's t-test. **c** An image of a *Dictyostelium discoideum* cell expressing RBD_{Raf1}-RFP. The spontaneous dynamics of Ras-GTP was analyzed by measuring the fluorescence intensity along the cell membrane over time to generate a kymograph. **d** Representative kymographs showing traveling waves of Ras-GTP in RasGEF OE strains. **e** Four patterns in the membrane localization of RBD_{Raf1}-RFP. The excitability increases from left to right as the amount of Ras-GTP on the cell membrane increases. Scale bars, 5 μm. Representative images from 3 independent experiments are displayed. **f** Fraction of cells showing each pattern: no domain (*blue*), transient domain (*green*), traveling wave (*magenta*), and uniform (*yellow*) after starvation for 3 h. Data are presented as the mean ± SD. n = 217, 168, 276, 209, 170, 119, 118, 222, 195, 116, 148, 178, 134, 200, 167, 231, 214, 298, 143, 163, 170, 184 and 349 cells from 3, 2, 3, 2, 2, 2, 2, 2, 2, 2, 2, 2, 2, 2, 2, 2, 3, 2, 3, 2, 2, 2, 2 and 3 independent experiments for WT, GEFA OE, GEFB OE, GEFC OE, GEFD OE, GEFE OE, GEFF OE, GEFG OE, GEFH OE, GEFK OE, GEFL OE, GEFM OE, GEFN OE, GEFO OE, GEFP OE, GEFR OE, GEFS OE, GEFT OE, GEFU OE, GEFV OE, GEFW OE, GEFX OE and GEFY OE, respectively. **g** Hierarchical clustering of RasGEFs based on the spontaneous dynamics of Ras-GTP in OE cells. Clusters 1 (*bottom*) through 5 (*top*) are arranged in descending Ras excitability. Colored squares indicate the features of RasGEFs in WT cells: high (*red*), middle (*orange*) or low (*yellow*) expression levels at the indicated time windows during development; phosphorylated (*blue*) or not phosphorylated (*pale blue*) upon cAMP stimulation; localized on the cell membrane with traveling waves (*violet*), uniformly on the cell membrane (*pink*) or throughout the cytoplasm (*pale pink*).

but decreased in the others (A/G/T/K/R) (Fig. 1f), with the fraction varying from 27.4 ± 4.0% to 82.4 ± 2.6% depending on the type of RasGEF overexpressed. The fraction of cells with no domain was negatively correlated with the traveling wave fraction, showing that wave generation is an indicator of the degree of excitability under caffeine-treated conditions. The mean domain size was larger in only the RasGEFB OE strain but smaller in many more (A/D/G/H/K/L/O/P/R/Y) compared with WT cells (Supplementary Fig. 2g and Supplementary Table 4). The mean period was shorter in the RasGEF OE strains (B/C/D/H/M/N/O/P/S/T/U/V/W/X/Y), and no strains showed a longer period compared with WT cells (Supplementary Fig. 2h and Supplementary Table 4).

We classified the 22 RasGEFs by hierarchical clustering into clusters for which overexpression altered the Ras dynamics in a similar manner. The domain sizes and periods of the Ras-GTP-enriched domain were determined from individual RasGEF OE cells, and corresponding heatmaps were obtained for each cell population (Supplementary Fig. 3). Based on a hierarchical clustering analysis of the heatmap, RasGEFs were grouped into five clusters and aligned so that the sum of the fractions of the traveling wave and uniform domain subpopulations increased from top to bottom (Fig. 1f, g). Clusters 1 and 5 showed the largest positive and negative effects on Ras excitability, respectively (Fig. 1g). RasGEFB/M/X/U in cluster 1 enhanced the excitability relatively strongly, while RasGEFT/K/R in cluster 5 suppressed the excitability (Fig. 1g). In cluster 1, endogenous RasGEFs showed a peak in their gene expressions at around 4 to 8 hours after starvation[63]. Furthermore, they were not phosphorylated by cAMP[64], and they localized to the cell membrane even without cAMP or functional F-actin, except for RasGEFM, as shown below. In cluster 5, endogenous RasGEFs also showed a peak in gene expressions at around 4 to 8 hours after starvation. However, they were phosphorylated by chemoattractant stimulation. RasGEFs in cluster 4 shared similar characteristics to those in cluster 5, whereas the RasGEFs in clusters 2 and 3 shared few common characteristics. Considering that *Dictyostelium* cells can exhibit random migration without cAMP but chemotaxis with cAMP extensively after 4 hours of starvation[6], we concluded that RasGEFs in cluster 1 likely promote spontaneous excitability, while those in cluster 5 likely suppress spontaneous excitability.

RasGEFX is primarily required for Ras excitability

To elucidate the contributions of RasGEFB/M/X/U in cluster-1 on the excitable dynamics of Ras, we prepared 4 SKO strains and 6 DKO stains, in which mScarlet-I-RBD_{Raf1} was expressed to observe the Ras-GTP-enriched domain[65] (Fig. 2a and Supplementary Movie 2). In conditions where excitability was enhanced with caffeine, no *gefX-* cells showed traveling waves, while 66.1 ± 5.2% of WT cells did (Fig. 2b and Supplementary Table 5). The fractions of other cells with *gefB*, *gefM* or *gefU* KO showed traveling waves was 85.2 ± 6.3%, 77.6 ± 1.9% and 73.4 ± 4.3%, respectively, but they were reduced to almost zero with the DKO of *gefX* (Fig. 2b). DKOs with other combinations of RasGEFB/M/U exhibited significant wave generation, with *gefB-/M-* and *gefB-/U-* cells especially exhibiting enhanced excitability (Fig. 2b). These results indicate that RasGEFX is required for the generation of traveling waves and that RasGEFB/M/U are suppressive of Ras excitability even though their overexpression enhances it (Fig. 1). These apparently inconsistent observations can be explained by RasGEFB/M/U acting competitively against RasGEFX in the activation of Ras and having weaker GEF activity than RasGEFX. Therefore, it is likely that RasGEFX fully enhances excitability in cells in which competitive *gefB*, *gefM* and *gefU* are knocked out.

We then observed spontaneous Ras-GTP dynamics in the KO and OE strains under conditions where excitability is not enhanced by caffeine. WT cells exhibited transient generations of the Ras-GTP-enriched domain (33.9 ± 9.4%) but little generation of traveling waves (Fig. 2c, d, Supplementary Table 6 and Supplementary Movie 2). RasGEFB/M/U/X OE cells enhanced Ras excitability even without caffeine, showing the excitatory roles of cluster-1 RasGEFs when highly expressed (Supplementary Fig. 4a, b and Supplementary Table 7). Cells missing RasGEFX (*gefX-*, *gefB-/X-*, *gefU-/X-* and *gefM-/X-*) showed impaired domain generation, consistent with the caffeine observations (Fig. 2c, d, Supplementary Table 6 and Supplementary Movie 2). On the other hand, the disruption of RasGEFB/M/U (*gefB-*, *gefM-*, *gefB-/M-*, *gefB-/U-* and *gefM-/U-*), in which RasGEFX is expected to be intact, tended to increase Ras excitability, in which traveling waves were often observed even without caffeine. These results indicate that RasGEFX is required for the spontaneous excitation generating the Ras-GTP-enriched domain, while RasGEFB/M/U are competitive with RasGEFX but can enhance the spontaneous excitability with their exogenous expression. Thus, RasGEFX is primarily responsible for spontaneous symmetry breaking in the Ras excitable system to generate an asymmetric Ras-GTP-enriched domain, while RasGEFB/M/U modulate the spatiotemporal dynamics.

RasGEFX is required for random cell motility in combination with RasGEFB/M/U

To evaluate the involvement of cluster-1 RasGEFB/M/U/X in spontaneous cell motility, we examined the motility of KO and OE cells in the absence of both caffeine and chemoattractants. In this condition, no RasGEFB/M/U/X SKO cells showed serious defects in cell motility, although a sub-population of *gefX-* cells exhibited almost no migration and *gefM-* cells exhibited a relatively low migration speed (Fig. 3a, b, Supplementary Table 8 and Supplementary Movie 3). The mean migration speeds were 7.0 ± 3.5 μm/min for WT cells, 4.4 ± 3.5 μm/min for *gefX-*, 5.5 ± 2.9 μm/min for *gefM-*, 10.6 ± 4.8 μm/min for *gefB-* and 10.0 ± 3.4 μm/min for *gefU-* (Fig. 3b and Supplementary Table 8). RasGEFX DKO cells, including *gefB-/X-*, *gefU-/X-* and *gefM-/X-*, showed severely impaired spontaneous cell migration, whereas other DKO cells, including *gefB-/M-*, *gefB-/U-* and *gefM-/U-*, exhibited spontaneous

https://doi.org/10.1038/s41467-024-55389-2

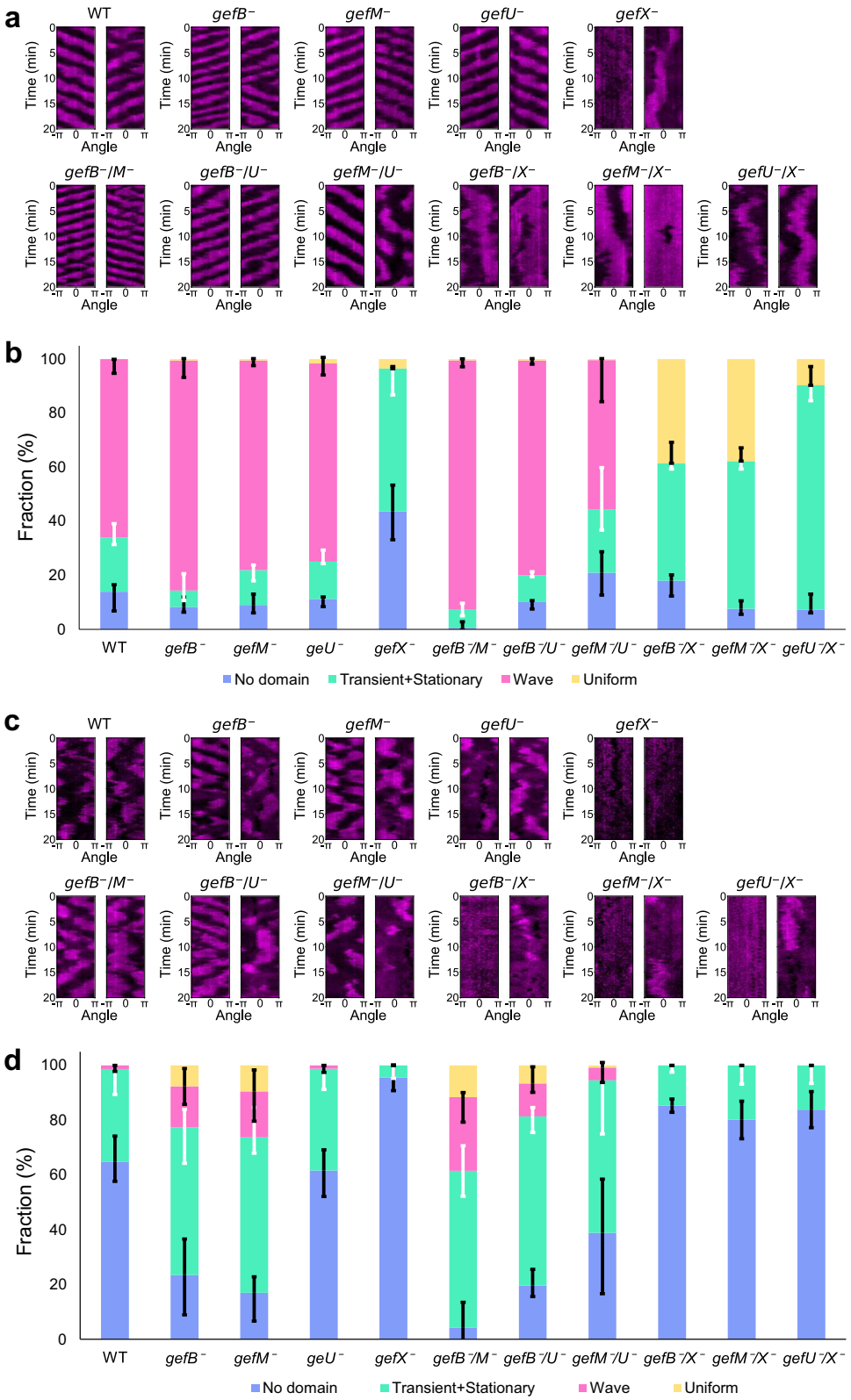

migration, albeit with slight defects (Fig. 3a, b). The mean square displacement (MSD) of the migration trajectories confirmed that the spontaneous cell motility depended on RasGEFX in combination with RasGEFB/M/U (Fig. 3c). The migration speed decreased in all OE strains compared to WT cells (Fig. 3d–f, Supplementary Table 8 and Supplementary Movie 3) due to the abnormal formation of pseudopods over the whole cell surface by over-activation of the excitable system. In addition, the overexpression of RasGEFU enhanced cell adhesion to substrates, consistent with previous reports of cGMP-binding protein D (GbpD), which is the same as RasGEFU[40,66] (Supplementary Fig. 4c). The hierarchical clustering analysis based on the Ras-GTP excitability with caffeine showed that the genetic disruption of RasGEFX (*gefX-*,

Fig. 2 | RasGEFX is primarily required for Ras excitability. a, b Ras-GTP dynamics in RasGEF KO strains in the presence of caffeine. Cells were starved for 3 h. **a** Representative kymographs of mScarlet-I-RBD$_{Raf1}$. **b** Fraction of cells showing each pattern: no domain (*blue*), transient domain and stationary domain (non-oscillatory domains; *green*), traveling wave (*magenta*), uniform (*yellow*). Data are presented as the mean ± SD. n = 200, 191, 210, 217, 286, 213, 223, 202, 314, 225, 271 cells from 3, 2, 2, 2, 2, 2, 2, 3, 2, 2, and 2 independent experiments for WT, *gefB-*, *gefM-*, *gefU-*, *gefX-*, *gefB-/M-*, *gefB-/U-*, *gefM-/U-*, *gefB-/X-*, *gefM-/X-* and *gefU-/X-*, respectively. **c, d** Ras-GTP dynamics in RasGEF KO strains in the absence of caffeine. Cells were starved for 3 h. **c**, Representative kymographs of mScarlet-I-RBD$_{Raf1}$. **d** Fraction of cells showing each pattern: no domain (*blue*), non-oscillatory domains (*green*), traveling wave (*magenta*), uniform (*yellow*). Data are presented as the mean ± SD. n = 87, 105, 119, 65, 121, 71, 85, 87, 166, 123 and 123 cells from 3, 5, 6, 4, 4, 3, 3, 6, 4, 4 and 4 independent experiments for WT, *gefB-*, *gefM-*, *gefU-*, *gefX-*, *gefB-/M-*, *gefB-/U-*, *gefM-/U-*, *gefB-/X-*, *gefM-/X-* and *gefU-/X-*, respectively.

gefB-/X-, *gefU-/X-* and *gefM-/X-*) significantly reduced the traveling wave generation (Fig. 3g, and Supplementary Fig. 4d). Even in the absence of caffeine, the cluster in which RasGEFX gene was disrupted showed impaired domain generation. Furthermore, the DKO strains in this cluster exhibited a significant decrease in the migration speed. Conversely, the strains in the other cluster with intact RasGEFX exhibited relatively higher motility. These results indicate that RasGEFX plays a key role in the spontaneous signal generation for basal cell motility and RasGEFB/M/U in cluster-1 are required with RasGEFX to achieve normal cell migration.

RasGEFX and RasGEFB co-localize in the Ras-GTP-enriched domain to generate traveling waves

To reveal the mechanisms by which cluster-1 RasGEFs underlie Ras excitability, we examined the subcellular localization of GFP-tagged RasGEFs. Among the 25 RasGEFs, only RasGEFB/U/X in cluster-1 and RasGEFW in cluster-3 exhibited obvious localization to the plasma membrane (Supplementary Fig. 5). RasGEFB/U/X have no transmembrane domain, suggesting dynamic shuttling between the membrane and the cytosol; in contrast, RasGEFW has a transmembrane domain[38]. Among cluster-1 RasGEFs, RasGEFX and RasGEFB exhibited traveling waves co-localizing with Ras-GTP, and cross-correlation functions between each RasGEF and Ras-GTP revealed a tight coincidence of localization and oscillatory dynamics with almost no time lag (Fig. 4a, b and Supplementary Movie 4), suggesting their direct involvement in traveling wave generation. Consistently, RasGEFB/X-GFP were observed in the cytosol but not on the membrane when the cells had no Ras-GTP-enriched domain. RasGEFU localized almost uniformly to the membrane and did not exhibit traveling waves, while RasGEFM was observed throughout the cytoplasm (Fig. 4c, d and Supplementary Movie 4), suggesting uniform modulation of GEF activity on the membrane and in the cytosol by RasGEFU and RasGEFM, respectively.

To further examine how cluster-1 RasGEFs regulate the spatiotemporal dynamics of the Ras-GTP-enriched domain, the oscillation periods and the spatial sizes of the traveling waves were characterized by the expression level of RasGEFB/M/U/X. Increasing the expression of RasGEFX-GFP shortened the oscillation period of traveling waves but without any obvious correlation with the spatial size of the Ras-GTP-enriched domain (Fig. 4e–g). On the other hand, increasing the expression of RasGEFB-GFP resulted in larger domains with no obvious correlation with the oscillation period (Fig. 4e–g). Neither the oscillation period nor the size was dependent on the expression level of RasGEFU-GFP or RasGEFM-GFP (Fig. 4e–g). These results indicate that RasGEFX and RasGEFB regulate the temporal and spatial dynamics of Ras excitability, respectively. Because RasGEFX is responsible for the excitable firing and traveling wave generation without and with caffeine, respectively, RasGEFX triggers spontaneous symmetry breaking as a temporal regulator in the excitable system to generate an asymmetric signal for basal cell motility. RasGEFB, on the other hand, modulates the spatial properties of the Ras-GTP-enriched domain in the excitable system. RasGEFM and RasGEFU hardly affected the spatiotemporal characteristics in Ras excitability in the absence of a functional actin cytoskeleton, but they could increase subpopulations of excited cells when they were overexpressed (Fig. 1).

RasGEFX and RasGEFB regulate actin cytoskeleton-dependent protrusion dynamics in a different manner

We further examined the subcellular localization of cluster-1 RasGEFs under the presence of a functional actin cytoskeleton without caffeine to reveal how RasGEFs regulate actin cytoskeleton-dependent cellular processes such as pseudopod formation and macropinocytosis[21,53–56]. RasGEFX-GFP and RasGEFB-GFP co-localized in the Ras-GTP-enriched domain at leading-edge pseudopods, while RasGEFU-GFP and RasGEFM-GFP showed uniform localization along the whole membrane and in the cytosol, respectively (Fig. 5a and Supplementary Movie 5). That is, a functional actin cytoskeleton did not cause remarkable changes in the localization of cluster-1 RasGEFs. However, a characteristic morphological change was observed due to the cytoskeletal dynamics, especially in RasGEFX-GFP- and RasGEFB-GFP-expressing cells. RasGEFX-GFP-expressing cells often showed multiple pseudopods or macropinocytic cups in which RasGEFX-GFP was localized (Fig. 5a). RasGEFB-GFP-expressing cells showed macropinocytosis less frequently than RasGEFX-GFP-expressing cells; instead, they often had multiple lamellipodia-like pseudopods or one larger pseudopod (Fig. 5a). RasGEFU-GFP-expressing cells showed increased adhesion to the substrates and thus less motility as their expression increased (Fig. 5a).

Because RasGEFX and RasGEFB regulate the oscillations temporally and sizes spatially of Ras-GTP-enriched domains without an actin cytoskeleton, respectively, we analyzed the frequency and size of the actin-dependent protrusions in starved cells under physiological conditions (Fig. 5b, c). Here, lamellipodia-like protrusions and macropinocytosis-associated protrusions were distinguished. *gefX-* cells showed suppressed protrusion formation (Fig. 5d, Supplementary Table 9 and Supplementary Movie 5). RasGEFX overexpression in *gefX-* cells markedly promoted the formation of both pseudopods and macropinocytic cups but suppressed pseudopod size. In contrast, RasGEFB/M/U-deficient mutants (*gefB-*, *gefM-* and *gefU-*), in which RasGEFX is expected to be intact, showed more frequent pseudopod formation than *gefX-*, while the macropinocytic cup formation was hardly changed compared to WT cells. The overexpression of RasGEFB in *gefB-* cells significantly expanded the area of the pseudopod without changing the frequency of the pseudopod formation (Fig. 5d, Supplementary Table 9 and Supplementary Movie 5). These observations are consistent with the roles of RasGEFX and RasGEFB as temporal and spatial regulators in the Ras excitable system, respectively. *gefU-* cells showed greatly enhanced pseudopod formation due to the increased motility caused by reduced adhesion, while RasGEFU overexpression in these cells led to a large pseudopod and also less motility (Fig. 5d and Supplementary Table 9). RasGEFM overexpression in *gefM-* cells enhanced the formation of pseudopods of normal size slightly, while both *gefM-* cells and RasGEFM OE in *gefM-* cells exhibited no obvious changes in the macropinocytic cup formation (Fig. 5d and Supplementary Table 9). Thus, RasGEFX primarily triggers spontaneous Ras excitation to generate a signal for pseudopod formation for basic cell motility under no chemoattractant and to induce macropinocytosis with increasing expression even when the cells are starved. This spontaneous symmetry breaking in the Ras excitable system leads to the anterior-posterior polarity of motile cells. On the other hand, RasGEFB and RasGEFU modulate the polarity by regulating the sizes of the Ras-GTP-enriched domain and the cell adhesion, respectively.

https://doi.org/10.1038/s41467-024-55389-2

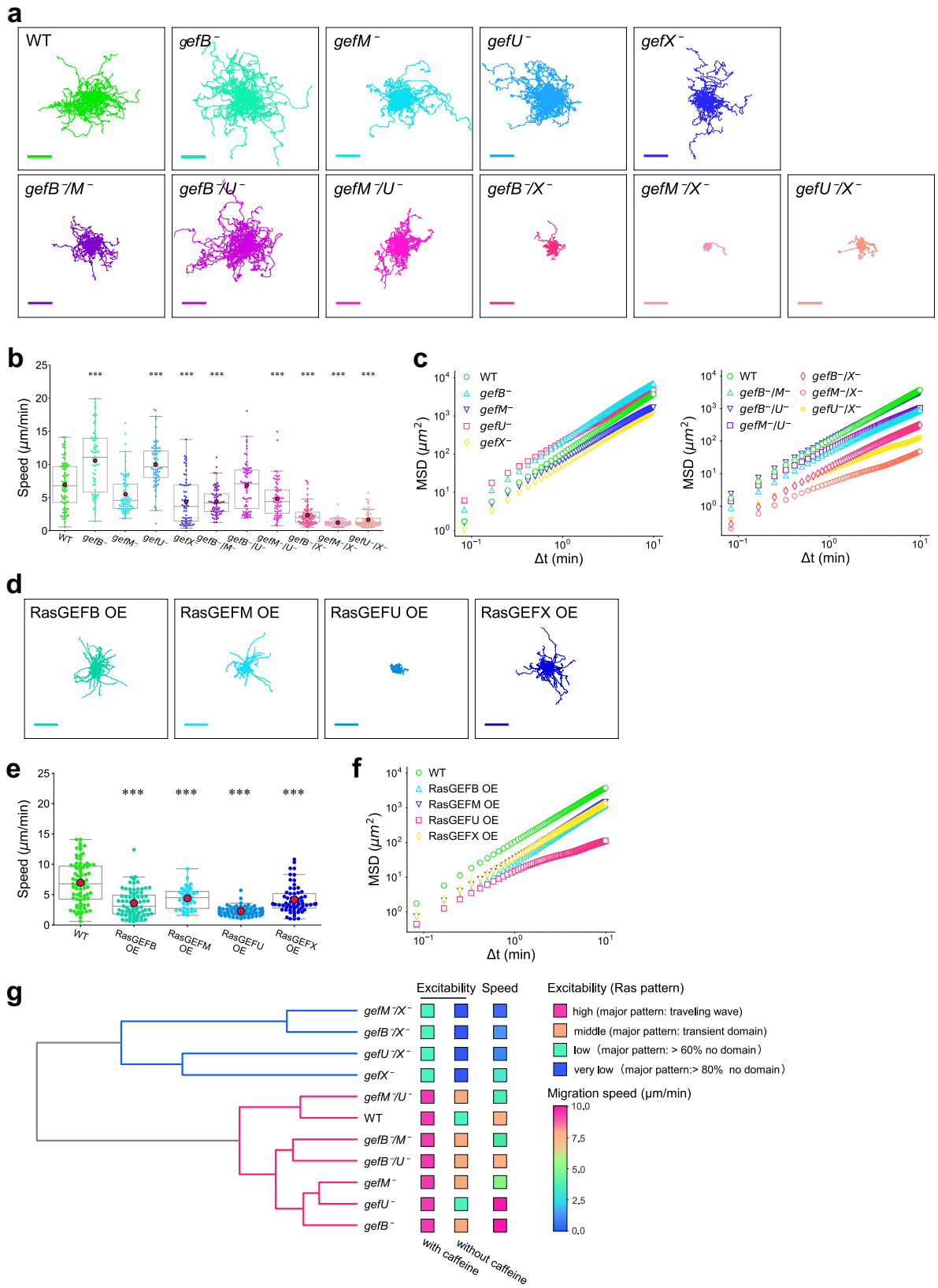

The involvement of RasGEFX in macropinocytosis was further examined in vegetative cells. RasGEFX-GFP was clearly localized to the macropinocytic cups when expressed in *gefX*- cells, where macropinosomes were visualized with the fluid-phase marker tetramethylrhodamine isothiocyanate (TRITC)-dextran (Fig. 6a). The rate of TRITC-dextran uptake was remarkably reduced in *gefX*- cells, but in RasGEFX OE cells it was slightly higher level than in WT cells (Fig. 6b). The frequency of the macropinocytic cup formation was also enhanced in RasGEFX OE cells (Fig. 6c and Supplementary Table 10). In contrast, RasGEFB OE cells, which were widely distributed on the plasma membrane, showed a slight decrease in macropinocytosis (Fig. 6a–c and Supplementary Table 10). No obvious changes were

Fig. 3 | RasGEFX, RasGEFB, RasGEFU and RasGEFM are important for efficient spontaneous motility. a–c Statistical analysis of spontaneous motility by RasGEF KO strains. Cells were starved for 3 h. **a** Trajectories of spontaneously migrating KO cells. WT, $n = 77$ cells; *gefB-*, $n = 67$ cells; *gefM-*, $n = 77$ cells; *gefU-*, $n = 70$ cells; *gefX-*, $n = 65$ cells; *gefB-/M-*, $n = 66$ cells; *gefB-/U-*, $n = 66$ cells; *gefM-/U-*, $n = 62$ cells; *gefB-/X-*, $n = 70$ cells; *gefM-/X-*, $n = 65$ cells; *gefU-/X-*, $n = 66$ cells. Scale bars, 100 μm. **b** Speed of spontaneous migration using data from 2 independent experiments in (**a**). Closed circles in magenta show mean values. The box-and-whisker plots show the median as horizontal lines, the first and third quartiles as box ends, and the whiskers as lower limit and upper limit values. *** $p < 0.001$; two-sided Dunnett's test. **c** MSD calculated for each KO strain. **d–f** Statistical analysis of spontaneous motility by RasGEF OE strains. Cells were starved for 3 h. **d** Trajectories of spontaneously migrating OE cells. RasGEFB OE, $n = 75$ cells; RasGEFM OE, $n = 39$ cells; RasGEFU OE, $n = 66$ cells; RasGEFX OE, $n = 65$ cells. Scale bars, 100 μm. **e** Speed of the spontaneous migration. using data from 2 independent experiments in (**d**). Closed circles in magenta show mean values. The box-and-whisker plots show the median as horizontal lines, the first and third quartiles as box ends, and the whiskers as lower limit and upper limit values. *** $p < 0.001$; two-sided Dunnett's test. **f** MSD calculated for each OE strain. **g** Hierarchical clustering of RasGEF KO strains based on the spontaneous dynamics of Ras-GTP with caffeine. Clusters 1 (*bottom*) and 2 (*top*) are arranged in descending Ras excitability. Colored squares indicate the features of RasGEF KO strains: high (*pink*), middle (*orange*), low (*cyan*) or very low (*blue*) fractions of domain patterns; migration speed is referred to the color bar.

observed in the macropinocytosis of vegetative RasGEFU/M KO or OE cells (Fig. 6a–c and Supplementary Table 10). The same was true for pseudopod formation for all four RasGEFs. Additionally, we found that the growth rate of *gefX-* cells was reduced compared to WT cells. Furthermore, we found that the expression level of RasGEFX was not correlated to the rate of phagocytosis (Supplementary Fig. 6a). Similarly, RasGEFX was not essential for multicellular development through intercellular signaling with cAMP oscillations (Supplementary Fig. 6b–d). Other RasGEFs in cluster-1 seemed to play only a partial role in modulating the phagocytosis rate and developmental timing, although RasGEFM affected the efficiency of phagocytosis (Supplementary Fig. 6a). Thus, RasGEFX predominantly works for the spontaneous generation of the Ras-GTP-enriched signaling domain that directs actin cytoskeleton remodeling, a process effective for macropinocytosis in vegetative cells and for spontaneous migration in starved cells.

Cluster-1 RasGEFs are dispensable for cAMP-induced Ras activation and chemotaxis

To explore the possible roles of cluster-1 RasGEFs in cAMP signaling and chemotaxis, the response dynamics of Ras activity was examined by applying uniform cAMP stimulations. After stimulation with a sufficiently high concentration (10 μM), a transient membrane translocation of RBD_{Raf1}-RFP was observed, peaking at about 5 ~ 7 s in the WT strain (Fig. 7a). Similar responses were observed for *gefB-*, *gefM-*, *gefU-* and *gefX-* cells but with slight temporal differences in the cAMP-induced Ras activation (Fig. 7b). Dose response curves from 1 pM to 10 μM revealed the mutant cells responded similarly to WT cells (Fig. 7c). Therefore, these RasGEFs are unlikely necessary for cAMP-induced Ras activation, suggesting the involvement of other RasGEFs in cAMP signaling. Notably, *gefX-* cells were significantly less responsive to cAMP at 1 nM than the other KO strains, suggesting that the spontaneous enhancement of Ras excitability by RasGEFX is essential for a response to low cAMP concentrations, as described later in more detail.

Chemotaxis toward cAMP was examined by introducing a micropipette filled with 10 μM cAMP (Fig. 7d). Chemotaxis was observed in all KO strains, as evident by the trajectories of cell migration (Fig. 7e and Supplementary Movie 6). The migration speeds for almost all KO strains were faster than those in the absence of cAMP, showing the chemokinetic effects of cAMP on cluster-1 RasGEF-deficient mutants, although *gefB-* and *gefU-* cells migrated at nearly maximal speed without cAMP and thus no obvious enhancement with cAMP (Fig. 7f, g and Supplementary Table 11). The chemotactic index, a measure of chemotactic accuracy, showed no severe defects for most mutants when compared with WT (0.65 ± 0.28) (Fig. 7h, i and Supplementary Table 11). *gefB-/M-* cells showed enhanced chemotaxis efficiency (0.73 ± 0.23). Four exceptions for the defective chemotaxis were *gefX-* (0.48 ± 0.37), *gefU-* (0.54 ± 0.31), *gefM-/U-* (0.47 ± 0.33) and *gefU-/X-* (0.34 ± 0.31) (Fig. 7h, i and Supplementary Table 11), consistent with previous reports that RasGEFU is involved in chemotactic signaling via Rap1 activation[40,66]. The genetic disruption of RasGEFX, as seen in *gefX-*, *gefB-/X-*, *gefU-/X-* and *gefM-/X-* cells, impaired basic and random cell motility severely without external cAMP (Fig. 3 and Fig. 7g), but the mobility was recovered in all cases as directional motility with cAMP stimulation, albeit with defects (Fig. 7f–i). These results indicate that RasGEFB/M/U/X are not necessary for regulating the directionality of cell migration under cAMP gradients and that other RasGEFs may enhance the directional motility instead. Rather, cluster-1 RasGEFs are essential for the basal cell motility that arises independently of chemotactic signaling from environmental guidance cues.

We further examined the roles of RasGEFX in chemotaxis because *gefX-* cells were less responsive to low cAMP concentrations in Ras excitability and had inefficient chemotaxis to cAMP as seen in the chemotactic index (Fig. 7c, h, i). RasGEFX enhanced the response at a low concentration range of cAMP gradients. Small population assays, where the cells were allowed to migrate on the agar surface toward droplets containing known concentrations of cAMP, revealed the defective response of *gefX-* cells at low cAMP concentration ranges, while other single KO cells, including *gefB-*, *gefM-* and *gefU-*, exhibited wide-range chemotaxis[67,68] (Fig. 7j). The chemotactic index was also reduced in *gefX-* under a shallow gradient made by a micropipette that was filled with 10 μM cAMP and located far from the cells (Fig. 7k). Thus, basal Ras excitability achieved by RasGEFX before chemoattractant stimulation is critical for improving the chemotaxis efficiency at low cAMP concentration range.

Discussion

Excitable systems have been identified as key signaling networks for random cell migration[11,69]. They cause Ras-GTP to self-organize, thus generating the signaling domain on the membrane for cell motility[23,28,33,34]. Herein, we found that RasGEFX is primarily required for the spontaneous generation of the Ras-GTP-enriched domain and for basal cell motility (Figs. 1–3). RasGEFB/M/U work as regulators of the spontaneous dynamics and are required in combination with RasGEFX for random cell migration (Figs. 1–3). RasGEFX and RasGEFB regulate temporally and spatially the Ras excitability and the cytoskeletal dynamics for cell migration, respectively, while RasGEFU and RasGEFM regulate cell adhesion and migration speed, respectively (Figs. 4, 5). RasGEFX also regulates macropinocytosis when the cells are in the vegetative stage (Fig. 6). Finally, RasGEFB/M/U/X are dispensable for chemotactic signaling (Fig. 7). These findings indicate that a specific set of RasGEFs constitutes spontaneous signal generators for driving the random cell motility that operates independently of external chemotactic signaling.

Based on the different and combinatory roles of RasGEFX and RasGEFB/M/U determined experimentally (Figs. 2–5), we propose a model for the spontaneous excitable dynamics of Ras and cell motility regulation as follows. RasGEFX primarily triggers the spontaneous excitation, which defines the temporal properties of the Ras-GTP-enriched domain such as the firing frequency and the oscillation period. RasGEFB regulates the spatial properties of the Ras-GTP-enriched domain such as the domain size. RasGEFM and RasGEFU are

https://doi.org/10.1038/s41467-024-55389-2

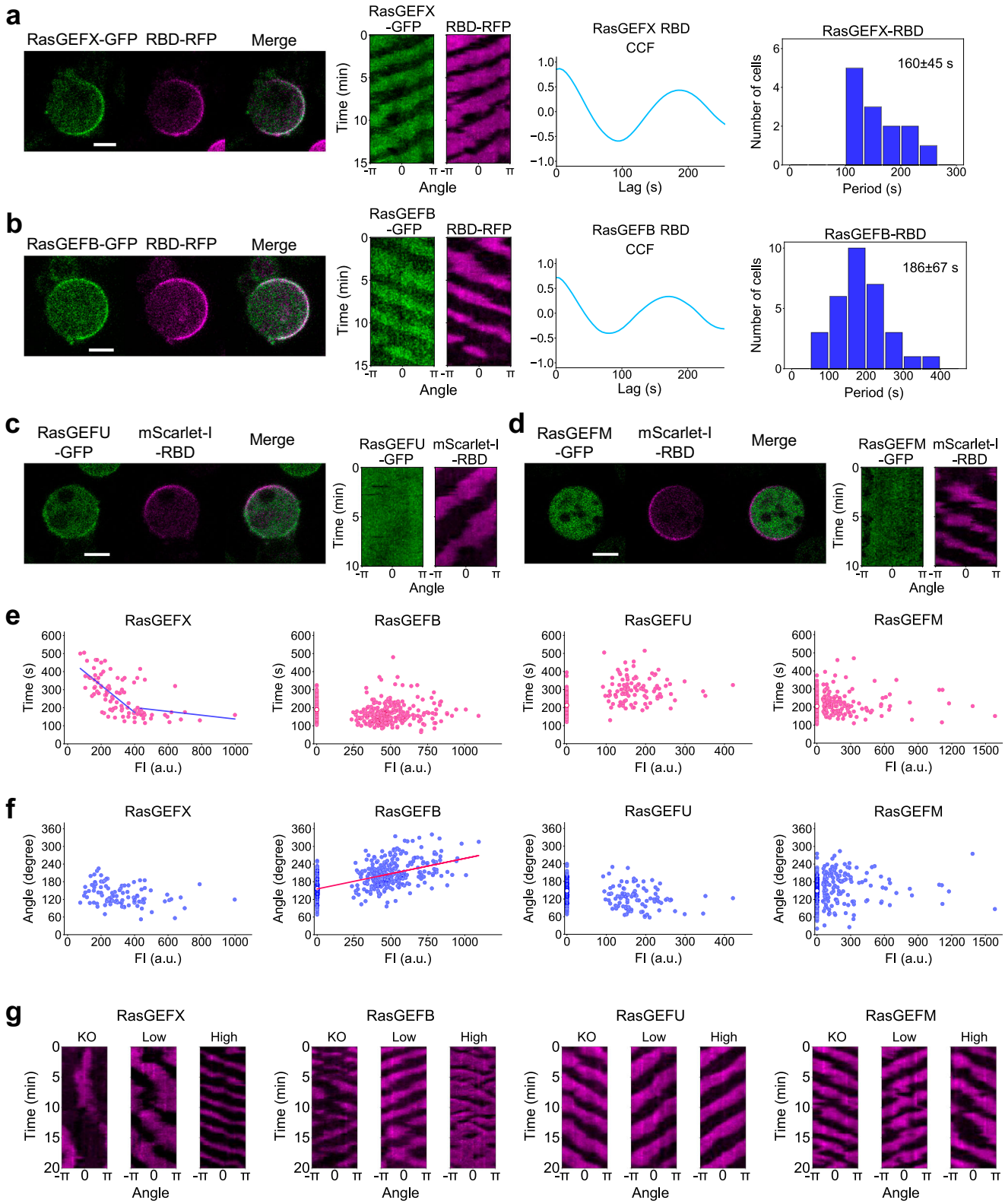

likely to modulate spontaneous excitability, and they can increase subpopulations of excited cells with their overexpression. For cell motility through remodeling of the actin cytoskeleton, RasGEFX and RasGEFB regulate the frequency of the protrusion formation and protrusion size, respectively, and thus the spatiotemporal dynamics of actin cytoskeleton-dependent protrusions are diverse and depend on the expression levels of these two RasGEFs. For example, RasGEFB overexpression can cause a transition from amoeboid migration to keratocyte-like gliding with a fan-shape (Supplementary Video 5). Such a transition in the motility mode has been documented with changes in the spatiotemporal dynamics of the excitable system[70]. In addition, RasGEFX overexpression promoted macropinocytosis, but no such promotion was observed for RasGEFB overexpression, suggesting their different roles in regulating cytoskeletal dynamics. Because RasGEFX and RasGEFB share a common RasGEF domain but differ in other regions, including Ser/Thr protein kinase for RasGEFX

Fig. 4 | RasGEFX and RasGEFB co-localize with Ras-GTP traveling waves. a–d Co-localization analysis of RasGEFX (**a**), RasGEFB (**b**), RasGEFU (**c**) and RasGEFM (**d**) with Ras-GTP. Cells were starved for 3 h. **a, b** Representative images of RasGEFX-GFP (**a**) and RasGEFB-GFP (**b**) with RBD_{Raf1}-RFP expressed in the respective RasGEF KO strains (*left*); representative kymographs (*middle left*); cross-correlation functions (CCFs) between RasGEF and RBD_{Raf1} (*middle right*); and the statistical distributions of the period estimated using the CCFs (*right*). RasGEFX, $n = 13$ cells; RasGEFB, $n = 30$ cells. **c, d**, Representative images of RasGEFU-GFP (**c**) and RasGEFM-GFP (**d**) with mScarlet-I-RBD_{Raf1} expressed in the respective RasGEF KO strains (*left*) and kymographs (*right*) from 3 independent experiments. **e, f** Relationships between the period (**e**) and domain size (**f**) of the Ras-GTP-enriched domain with the expression level of RasGEF quantified in the RasGEF KO strains with (fluorescence intensity (FI) > 0) or without (FI = 0) RasGEF-GFP expression. Closed circles represent the quantification in a single cell (*gefX-*, $n = 97$ cells; GEFB-GFP/*gefB-*, $n = 267$ cells; *gefB-*, $n = 132$ cells; GEFU-GFP/*gefU-*, $n = 101$ cells; *gefU-*, $n = 160$ cells; GEFM-GFP/*gefM-*, $n = 132$ cells; *gefM-*, $n = 163$ cells). Open circles represent the means of KO cells. **g** Representative kymographs of RBD_{Raf1}-RFP or mScarlet-I-RBD_{Raf1} without ("KO"), with low ("Low"), or with high expression ("High") of RasGEF-GFP in the respective RasGEF KO cells. Scale bars, 5 μm.

(Supplementary Fig. 3c), they may share regulatory functions for Ras excitability but also have other signaling functions for cell migration and macropinocytosis. As reported previously, RasGEFU (or GbpD) is involved in Rap1 activation and regulates cell adhesion[40]. Consistently, RasGEFU overexpression induced widely spread pseudopods, which adhere more strongly to the substrate leading to less efficient cell migration (Figs. 3 and 5). Given that spontaneous cell migration requires concerted regulation of the actin cytoskeleton and adhesion without external guidance cues, RasGEFB/U/X may contribute to the internal coordination by their common RasGEF functions in the excitable Ras system and their differential functions in the motile system. Previous reports show that RasGEFM is required for the activation of adenylyl cyclase for cAMP relay and multicellular development[71]. In our experimental conditions, neither cAMP relay nor development were affected by the disruption of RasGEFM (Supplementary Fig. 6). Both the knockout and overexpression of RasGEFM caused reduced motility and enhanced phagocytosis (Fig. 3 and Supplementary Fig. 6a), suggesting that RasGEFM may contribute to efficient migration and phagocytosis at appropriate expression levels.

Positive feedback mechanisms are required to amplify signals for the all-or-none response in excitable systems[30,69,72–75]. The co-localization of RasGEFB and RasGEFX with the Ras-GTP-enriched domain on the membrane suggests that the recruitment of RasGEFB and RasGEFX to the membrane depends on Ras-GTP and/or some factors localized in the Ras-GTP-enriched domain (Fig. 4), further suggesting positive feedback between RasGEFX/B and Ras-GTP. RasGEFX has a GEF_N domain (REM domain) that is homologous to that of mammalian SOS in the Ras/MAP kinase pathway[76,77] (Supplementary Fig. 4c). Extensive structural and biochemical analyses of SOS have revealed positive-feedback loops, in which the GEF_N domain of SOS can bind to Ras-GTP and allosterically enhance the activity of its GEF domain, leading to modification of the basal GDP/GTP exchange rate to favor Ras-GDP[78–81]. This mechanism can constitute an amplifying mechanism for Ras activation locally on the membrane. RasGEFX has a Ser/Thr kinase domain that SOS does not, which may be required for RasGEFX-specific functions that are not present in SOS. Finally, RasGEFB has a common RasGEF domain but no other recognizable signaling domains[38]. More studies are needed to understand the positive-feedback mechanisms for the excitable systems in eukaryotic chemotaxis, especially for the spontaneous generation of the Ras-GTP-enriched domain.

We found that the same Ras excitable system provides a basis for the formation of macropinocytic cups and pseudopods (Figs. 5 and 6). Both are self-organized structures generated locally on the membrane through remodeling of the actin cytoskeleton without extracellular asymmetric cues. Previous studies have shown that Ras and its regulators, including RasG/S, RasGAP, and NF1, regulate fluid uptake by macropinocytosis, where RasGEFF, RBD_{Raf1} and PI(3,4,5)P3 accumulate at the macropinocytic cups[21,44,50–52], suggesting some shared molecular mechanisms with pseudopodia formation. While vigorous macropinocytosis can be observed in the vegetative stage of *Dictyostelium* cells, the frequency gradually reduces upon starvation and instead the cells gain pseudopod-dependent basal motility[11,21,50,53–58]. Therefore, the Ras excitable system may remodel the actin cytoskeleton differently depending on the state of the cell: macropinocytic cups and pseudopods are formed at the Ras-GTP-enriched domain on the membrane of vegetative and starved cells, respectively, using the common RasGEFX-dependent mechanisms and the corresponding molecular mechanisms. RasGEFB can enhance pseudopod formation but suppress macropinocytic cup formation, suggesting the involvement of RasGEFB in switching between the two structures[82] (Fig. 5). In mammalian cells, although small GTPases, such as Rac1 and Cdc42, are involved in macropinocytosis, and Rac1 GEFs, such as DOCK1 and TIAM1, have been identified[83], RasGEFs have not been well documented.

Our observation that RasGEFB/M/U/X are not required for cAMP-induced Ras activation or chemotaxis may be explained partly by the four parallel signaling pathways (RasG/PI3K, RasC/TorC2, Rap1/sGC, and PLA2) for chemotaxis. Even if RasGEFB/M/U/X mediate directly the chemotactic signals via these pathways[84], SKO and DKO cells can exhibit chemotaxis if the other pathways maintain their function. In addition to this robust network structure for chemotaxis, because RasGEFA/G/K/R/T in clusters 4 and 5 are phosphorylated by chemoattractant stimulation[64] and because RasGEFA/C/H/F/R/Q are involved in Ras/Rap activation upon cAMP stimulation[41,43,44], these RasGEFs may be involved in cAMP-induced Ras activation and chemotaxis. Thus, a mechanism of signal integration is envisioned by which different but overlapping sets of RasGEFs activate Ras/Rap for spontaneous and directed motility. The specificity of RasGEFB/M/U/X for Ras/Rap is crucial when elucidating the molecular mechanism underlying Ras excitability for spontaneous cell migration and chemotaxis.

Excitable systems provide a mechanism to generate a unified output from multiple input signals. Owing to this property, motile cells can choose one moving direction in various environmental cues, such as chemoattractants, electric fields, shear flow, pH, and O_2/CO_2, under the influence of internal states such as cell cycle and starvation[85–88]. The large number of RasGEFs and RasGAPs expressed in a single cell may reflect the need to integrate various external and internal signals to achieve cellular decision-making adaptable to complex environments with various motile modes[89,90]. The underlying mechanism is worth investigating to understand the cellular survival strategy. Recent evidence has revealed diverse patterns of cytoskeletal waves on the cell membrane in various biological systems that depend on small GTP-binding proteins, such as Ras, Cdc42, Rac and Rho, suggesting common mechanisms[91,92]. Applying the comprehensive dynamics analysis, we report here to a variety of excitable and oscillatory systems to clarify the molecular network, which will provide a novel perspective on the molecular mechanisms and signal integrations in living cells.

Methods

Cell strains

Dictyostelium discoideum WT Ax2 was used as the parental strain. All cell lines were grown in HL5 medium (Formedium, UK) supplemented with penicillin and streptomycin, 100 ng/mL folic acid and 5 ng/mL vitamin B12 at 21°C[93], except for those with *rapA* gene disruption (*rapA-*, *rasC-/rapA-*, *rasG-/rapA-* and *rasG-/C-/rapA-*), which were cultured with

https://doi.org/10.1038/s41467-024-55389-2

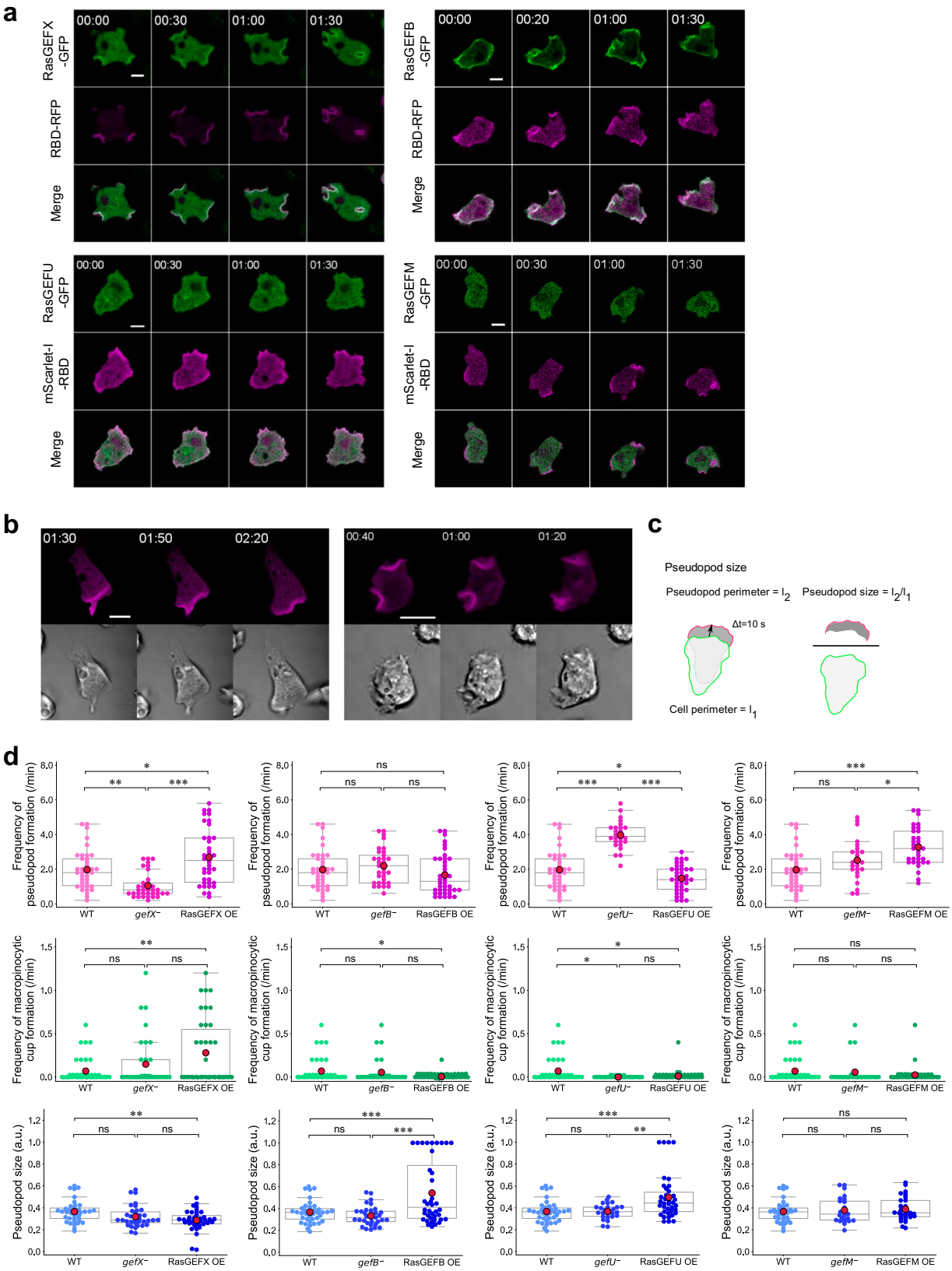

Escherichia coli B/r on a 5LP agar plate (Lactose 5.0 g, Bacto Peptone 5.0 g, Bacto agar 15.0 g)[94]. The strains overexpressing one of 25 RasGEFs in GFP-tagged form were generated by the electroporation of extrachromosomal plasmids for stable expression into the parental strain cells. The plasmids were generated by cloning RasGEF genes, which were amplified from WT genomic DNA by PCR using the primers listed in Supplementary Table 12, into the BglII site of pHK12neo. The transformants were selected and maintained under 20 μg/mL G418. The strains co-overexpressing RBD_{Raf1}-RFP or mScarlet-I-RBD_{Raf1} and RasGEF-GFP were generated by the electroporation of extrachromosomal plasmids for the stable expression of the Ras-GTP probe into RasGEF-GFP OE strains. The generation of the plasmid for

https://doi.org/10.1038/s41467-024-55389-2

Fig. 5 | RasGEFX and RasGEFB are respectively responsible for the temporal and spatial dynamics of protrusions. a Representative images of RasGEF KO cells expressing RasGEF-GFP and RBD_{Raf1}-RFP or mScarlet-I-RBD_{Raf1} with intact F-actin from 3 independent experiments. Scale bars, 5 μm. Time, min:sec. **b** Representative images of pseudopods (*left*) and macropinocytic cups (*right*) observed in WT cells expressing mScarlet-I-RBD_{Raf1} from 3 independent experiments. Confocal images (*top*) and DIC images (*bottom*) are shown. Scale bars, 10 μm. **c** Schematics for the quantification of pseudopod size. See Methods for details. **d** The frequency of the pseudopod formation (*top*), macropinocytic cup formation (*middle*) and the pseudopod size (*bottom*) in RasGEF KO and OE cells after 3 h of starvation. Closed circles represent the quantification in individual cells. $n = 38, 35, 38, 33, 40, 26, 38, 25$ and 33 cells from 5, 6, 5, 8, 3, 6, 6, 4 and 5 independent experiments for WT, *gefX-*, GEFX-GFP/*gefX-*, *gefB-*, GEFB-GFP/*gefB-*, *gefU-*, GEFU-GFP/*gefU-*, *gefM-* and GEFM-GFP/*gefM-*, respectively. Closed circles in magenta show mean values. The box-and-whisker plots show the median as horizontal lines, the first and third quartiles as box ends, and the whiskers as lower limit and upper limit values. * $p < 0.05$, ** $p < 0.01$, *** $p < 0.001$; ns, not significant; two-sided Tukey's test.

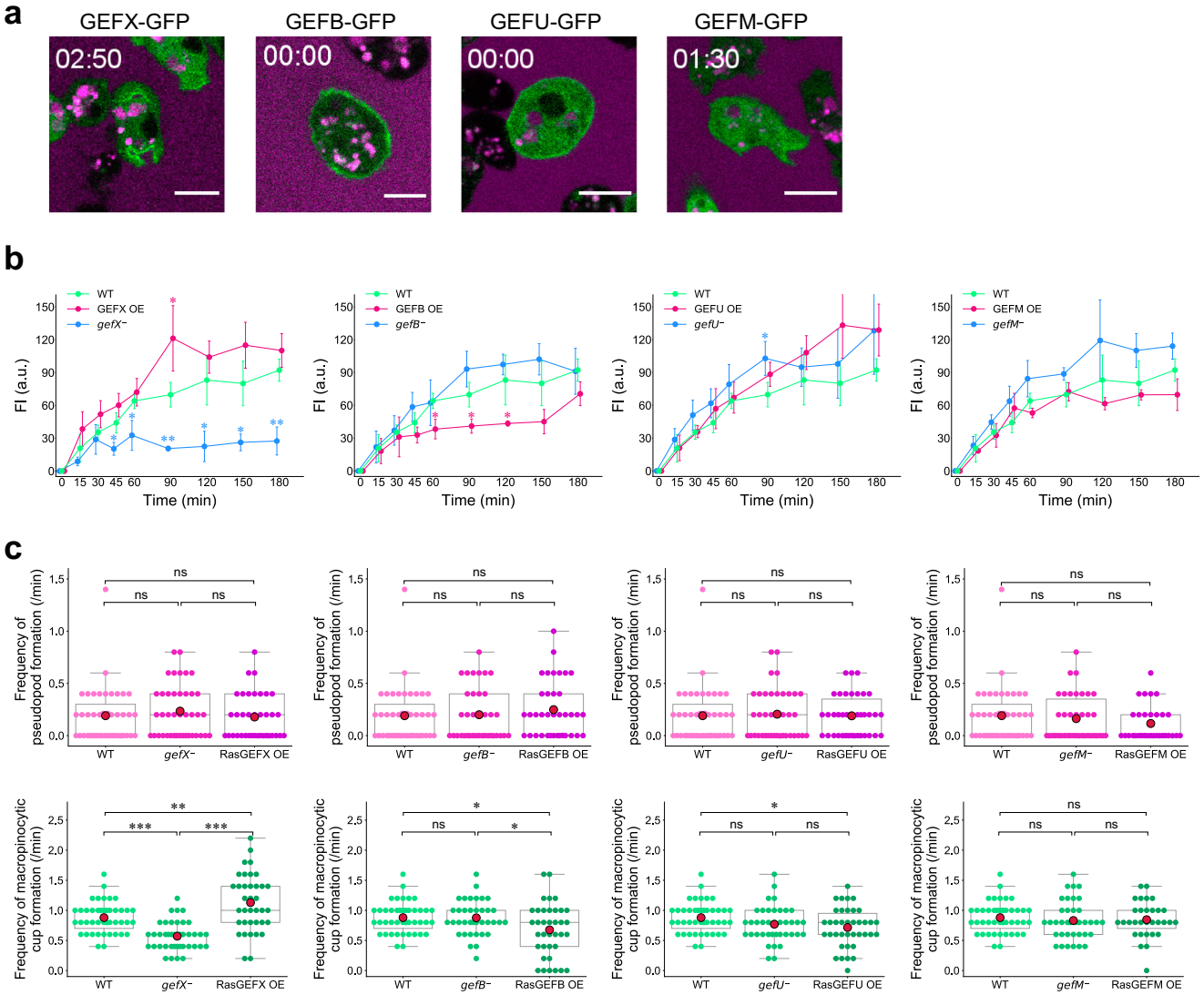

Fig. 6 | RasGEFX positively regulates macropinocytosis in vegetative cells. a Representative images of RasGEF KO cells expressing RasGEF-GFP and up-taking TRITC-dextran from 3 independent experiments. Scale bar, 10 μm. **b** Quantification of the fluorescence intensity of TRITC-dextran internalized in WT, RasGEF KO and OE cells in the vegetative state. Data are presented as the mean ± SD from 3 independent experiments. * $p < 0.05$, ** $p < 0.01$; two-sided Welch's *t*-test. **c** The frequency of the pseudopod formation (*top*) and macropinocytic cup formation (*bottom*) in RasGEF KO and OE cells in the vegetative state. Closed circles represent the quantification in individual cells $n = 43, 41, 37, 37, 37, 39, 38, 38$ and 31 cells from 3, 3, 4, 3, 3, 2, 3, 3 and 6 independent experiments for WT, *gefX-*, GEFX-GFP/*gefX-*, *gefB-*, GEFB-GFP/*gefB-*, *gefU-*, GEFU-GFP/*gefU-*, *gefM-* and GEFM-GFP/*gefM-*, respectively. Closed circles in magenta show mean values. The box-and-whisker plots show the median as horizontal lines, the first and third quartiles as box ends, and the whiskers as lower limit and upper limit values. * $p < 0.05$, ** $p < 0.01$, *** $p < 0.001$; ns, not significant; two-sided Tukey's test.

RBD_{Raf1}-RFP is described elsewhere[28]. The plasmid for mScarlet-I-RBD_{Raf1} pDM1208 was provided by the National Bio Resource Project (NBRP). The transformants were selected and maintained under 40 μg/mL Hygromycin B and 20 μg/mL G418. The expression of RBD_{Raf1}-RFP and mScarlet-I-RBD_{Raf1} was unstable, and the cells were observed microscopically within about 15 days of the electroporation.

The SKO strains *gefX-*, *gefB-*, *gefU-* and *gefM-* were generated using CRISPR/Cas9 by introducing extrachromosomal plasmids for the transient expression of both sgRNA and Cas9-NLS-GFP into the parental strain cells[95]. The plasmids were generated by cloning the target-site dsDNA fragments (Supplementary Table 12) into BpiI sites located between the isoleucine tRNA promoter and tracrRNA sequence in

pTM1285 by Golden Gate assembly[96]. The transformants were selected under 20 μg/mL G418 for 1 day and then maintained in the absence of G418. For cell cloning, we plated the cells on 5LP agar plates with Escherichia coli B/r and incubated them for 3–4 days until plaque formation. We transferred the individual plaques to 96-well plates (Thermo Fisher) containing HL5 in the absence of G418. The DKO strains *gefB-/M-*, *gefB-/X-* and *gefM-/X-* were generated by introducing the same CRISPR/Cas9 plasmids targeting *gefM*, *gefX* and *gefM* as described above into the strains of *gefB-*, *gefB-* and *gefX-*, respectively. The strains *gefB-/U-*, *gefM-/U-* and *gefU-/X-* were generated by homologous recombination targeting *gefU*[97]. Two fragments of RasGEFU gene, from bases 867 to 1641 and 2106 to 2993, were amplified by PCR using genomic DNA as a template and the primers listed in Supplementary Table 12, and the blasticidin S resistance (BSR) gene was

Fig. 7 | Chemotaxis and cAMP-stimulated Ras activation in RasGEF KO strains. **a** Time lapse images showing the transient membrane localization of RBD_{Raf1}-RFP in a WT cell in response to uniform 10 μM cAMP stimulation. Scale bar, 5 μm. Time, min:sec. **b** Quantification of the response in WT ($n = 67$ cells), *gefB-* ($n = 44$ cells), *gefM-* ($n = 33$ cells), *gefU-* ($n = 50$ cells) and *gefX-* ($n = 56$ cells) using mScarlet-I-RBD_{Raf1} and 10 μM cAMP. Cells were starved for 3 h. Data are presented as the mean ± SD from 2 independent experiments. **c** Fraction of responsive cells upon stimulation with 1 pM to 10 μM cAMP. $n > 30$ cells for each concentration (see Source Data). Data are presented as the mean ± SD from 2 independent experiments. The half-maximum effective concentrations are 1.34 nM (WT), 1.09 nM (*gefB-*), 0.69 nM (*gefM-*), 0.47 nM (*gefU-*) and 7.29 nM (*gefX-*). **d** Chemotaxis assay using a glass micropipette filled with 10 μM cAMP. Trajectories of WT cells for 20 min are shown. Scale bar, 100 μm. A representative image from 3 independent experiments is displayed. **e** Trajectories of cells after 5 h of starvation undergoing chemotaxis in response to 10 μM cAMP for 20 min. WT ($n = 121$ cells), *gefB-* ($n = 127$ cells), *gefM-* ($n = 125$ cells), *gefU-* ($n = 117$ cells), *gefX-* ($n = 117$ cells), *gefB-/M-* ($n = 140$ cells), *gefB-/U-* ($n = 127$ cells), *gefB-/X-* ($n = 119$ cells), *gefM-/U-* ($n = 140$ cells), *gefM-/X-* ($n = 129$ cells) and gefU-/X- ($n = 114$ cells). Scale bars, 100 μm. **f** Chemotaxis speed using data from 3 independent experiments in (**e**). Closed circles in magenta show mean values. The box-and-whisker plots show the median as horizontal lines, the first and third quartiles as box ends, and the whiskers as lower limit and upper limit values. *** $p < 0.001$; two-sided Dunnett's test. **g** Relationships between spontaneous motility speed (Fig. 3b) and chemotaxis speed (**f**) Data are presented as means ± SD. Letters indicate the disrupted genes. **h** Chemotactic index using data from 3 independent experiments in (**e**). Closed circles in magenta show mean values. The box-and-whisker plots show the median as horizontal lines, the first and third quartiles as box ends, and the whiskers as lower limit and upper limit values. * $p < 0.05$, *** $p < 0.001$; two-sided Dunnett's test. **i** Relationship between chemotaxis speed (**f**) and chemotactic index (**h**). Data are presented as the mean ± SD. Letters indicate the disrupted genes. **j** The chemotactic response of cell drops to different cAMP concentrations (1 nM to 1 mM) evaluated by the small population assay. Cells were starved for 5 h. $n = 36$ cell drops in each condition from 3 independent experiments. Data are presented as the mean ± SD. * $p < 0.05$, ** $p < 0.01$; two-sided Welch's *t*-test. **k** Chemotactic index of WT and *gefX*$^-$ cells undergoing chemotaxis in response to 10 μM cAMP at different distances (0–350 μm and >350 μm) from the micropipette tip. Closed circles in magenta show mean values. The box-and-whisker plots show the median as horizontal lines, the first and third quartiles as box ends, and the whiskers as lower limit and upper limit values. ** $p < 0.01$, *** $p < 0.001$; two-sided Welch's *t*-test.

inserted between them by fusion PCR. Fusion PCR was performed in 10 μL total volume using 1 ng of two fragments of RasGEFU gene, the fragment of BSR gene and 5 pmol of primerA and primerD (Supplementary Table 12). The fusion PCR conditions were as follows: heating to 94 °C for 2 min; 30 cycles of 94 °C for 30 s, 50 °C for 20 s and 68 °C for 4 min; followed by a final extension for 4 min. The transformants were selected under 10 μg/mL blasticidin S. We performed cloning with CRISPR-Cas9. *rasC-*, *rasG-*, *rapA-*, *rasC-/G-*, *rasC- rapA-*, *rasG- rapA-* and *rasC-/G- rapA-* were generated by CRISPR/Cas9 as described above. The dsDNA fragments of each target site are shown in Supplementary Table 12.

Electroporation of *Dictyostelium* cells

The cultured cells were collected by centrifugation at 500 × g for 2 min and resuspended at 1×10^7 cells/mL in H50 buffer (50 mM KCl, 20 mM HEPES, 10 mM NaCl, 5 mM $NaHCO_3$, 1 mM NaH_2PO_4, 1 mM $MgSO_4$, pH 7.0). A 100 mL cell suspension was mixed with 5 mg plasmid and incubated on ice for 5 min. The cell suspension was transferred to a cuvette with a 1-mm gap and set in an electroporator (BTX) to give a shock of 500 mV for 100 ms repeated 2 times at an interval of 5 s. The cell suspension was kept on ice for 2 min and transferred to a culture dish. After a 2-min incubation at 21 °C, 10 mL of HL5 medium was added to grow the cells at 21 °C. The drugs used for the selection were added 12 ~ 24 hours after the electroporation.

Confirmation of gene knockout

Genomic DNA was isolated from the transformants, and the nucleotide sequence at the target site was confirmed as follows. Cells were collected from plaques on 5LP agar plates and were resuspended in lysis buffer (200 mM Tris-HCL pH8.4, 500 mM KCl, 1.75 μM $MgCl_2$, 0.5% NP40, 20 μg/mL proteinase K and 20 μg/mL RNase). The suspension was incubated at 56 °C for 50 min and 95 °C for 10 min to inactivate proteinase K. A DNA fragment encompassing the target site was amplified by PCR using the lysate as a template, the primers listed in Supplementary Table 12, and SapphireAmp Fast PCR Master Mix (Takara). The PCR conditions were as follows: heating to 94 °C for 2 min; 35 cycles of 94 °C for 30 s, 50 °C for 45 s, and 68 °C for 1 min/kbp; followed by a final extension for 5 min. The amplified fragment was subjected to gel electrophoresis, where the band shift due to the insertion of the BSR cassette was confirmed in the case of homologous recombination and purified using a PCR purification kit (NEB), in which the nucleotide sequence was determined (Genewiz). We confirmed that the deletion or insertion of some bases by CRISPR/Cas9 led to an insertion of the stop codon in the coding sequence, in which the nucleotide sequence was determined (Genewiz) using the screening primers listed in Supplementary Table 12. *rapA-* prepared in this study exhibited a significant reduction of Rap1 activity, as detected using RalGDS-GFP, a commonly used reporter for activated Rap1, both before and after cAMP stimulation[98].

Cell preparation for microscopy

Cultured cells were starved as follows. The cells were washed three times with development buffer without Ca^{2+} or Mg^{2+} (DB−; 5 mM Na_2HPO_4 and 5 mM KH_2PO_4, pH 6.5) by centrifugation at 500 × *g* for 2 min. The cells were resuspended at 3.0×10^6 cells/mL in DB+ (5 mM Na_2HPO_4, 5 mM KH_2PO_4, 2 mM $MgSO_4$, 0.2 mM $CaCl_2$, pH 6.5), and 1 mL cell suspension was plated on a 35-mm dish (IWAKI). To observe subcellular localization and spontaneous motility, the cells were incubated for 3 h at 21 °C. To observe chemotaxis, the cells were incubated for 5 h at 21 °C. After the starvation period, the cells were washed twice with DB- and resuspended at 3.0×10^6 cells/mL in DB+ on ice until use. The gene knockout strains *rapA-*, *rasC-/rapA-*, *rasG-/rapA-* and *rasG-/C-/rapA-* were observed in the same manner without starvation.

Fluorescence microscopy

Laser scanning confocal microscopy (A1, Nikon) was performed on the treated cells described above. RFP and mScarlet-I tagged to RBD_{Raf1} were excited with a 561 nm laser (Coherent), and 570–620 nm fluorescence light was detected by a detector (A1-DU4, Nikon) equipped with the microscope. GFP tagged to RBD_{Raf1} and GFP tagged to RasGEFs were excited with a 488 laser (Coherent), and 500–550 nm light was detected by the detector. An emitted fluorescence was imaged with a 60x objective lens (CFI Apo TIRF 60X Oil, NA 1.49, Nikon).

To observe Ras-GTP dynamics in the presence of caffeine for RasGEF screening (Fig. 1), we utilized RBD_{Raf1}-RFP as a fluorescent probe for Ras-GTP. A 150 μL cell suspension was mixed with 150 μL DB+ containing 8 mM caffeine (Wako) and 20 μM latrunculin A (Sigma-Aldrich) and placed on a 35-mm glass bottom dish (12-mm glass in diameter; Iwaki). After the cells were allowed to adhere to the glass surface for 20 min, the images were acquired at a time interval of 5 s for 20 min.[14] To observe Ras-GTP dynamics in the absence of caffeine (Fig. 2), a 50 μL cell suspension was mixed with 100 μL DB+ and 150 μL DB+ containing 20 μM latrunculin A and placed on a 35-mm glass bottom dish, in which the cell density was reduced to 1/3 of the sample containing caffeine to suppress intercellular communication via secreted cAMP.

To observe Ras-GTP in the knockout strains of RasGEFB/U/M/X, we utilized mScarlet-I-RBD_{Raf1} since mScarlet-I is more stable and has higher fluorescence than RFP (Fig. 2). We utilized RBD_{Raf1}-RFP or

mScarlet-I-RBD_{Raf1} and RasGEF-GFP to observe Ras-GTP and RasGEF simultaneously in latrunculin A-treated cells, respectively (Fig. 4). The cell preparation and image acquisition were the same as described above. To examine the expression levels of RasGEF-GFP, a snapshot image of RasGEF-GFP at the beginning of the image acquisition was used (Fig. 4).

To observe Ras-GTP and RasGEF localization in migrating cells (Fig. 5), we utilized RBD_{Raf1}-RFP or mScarlet-I-RBD_{Raf1} and RasGEF-GFP, respectively. A 50 μL cell suspension was mixed with 250 μL DB+ and placed on a 35-mm glass bottom dish, and the cells were allowed to adhere to the glass surface for 20 min.[14] The images were acquired every 5 s for 5 min. To observe the response to cAMP (Fig. 7), the cell suspension was mixed with DB+ containing latrunculin A at a final concentration of 10 μM, and a 20 μL cell suspension was placed on a 35-mm glass bottom dish. Again, the cells were allowed to adhere to the glass surface for 20 min. The images were acquired every 1 s for 1 min. When 5 s passed after starting the image acquisition, 180 μL DB+ containing cAMP was added at a final concentration of 1 pM-10 μM.

We utilized RBD_{Raf1}-GFP to examine the membrane localization of RBD_{Raf1} in Ras/Rap-gene KO strains since mScarlet-I-RBD_{Raf1} and RBD_{Raf1}-RFP were not expressed stably in *rapA* KO strains (Fig. 1a, b and Supplementary Fig. 1a, b).

Cell migration imaging

Starved cells were washed twice with DB- and resuspended at 5.0×10^4 cells/mL in DB + . 300 μL cell suspension was placed on a coverslip (MATSUNAMI) that was first washed by sonication in 0.1 N KOH for 30 min and then 99.5% ethanol. The cells were allowed to adhere to the glass surface for 20 min. 1 mL DB+ was added, and the cells were allowed to settle for another 20 min. The cells were observed under an inverted microscope (IX71, Olympus) with a 20x objective lens (LCACHN20XPH, NA 0.4, Olympus). Images were acquired with a time-lapse camera (DS-2MBW, Nikon) every 5 s for 30 min. To examine chemotaxis, the concentration gradient of cAMP was generated using FemtoJet (Eppendorf): DB+ containing 10 μM cAMP was filled in a glass micropipette (Femtotips, Eppendorf) and released by applying pressure at 50 hPa.

cAMP oscillation and multicellular development

To analyze the period of cAMP oscillation during the early aggregation stage, cultured cells were washed three times with DB- and resuspended at 5.0×10^6 cells/mL in DB + . A 1 mL cell suspension was plated on 2% agar plate (Bacto-agar; dissolved in DB +), and excess liquid was allowed to evaporate. The cells were observed under an inverted microscope (IX71, Olympus) with a 5x objective lens (UPLFN4XPH, NA 0.13, Olympus). Images were acquired with a time-lapse camera (DS-2MBW, Nikon) every 30 s for 10 h. To observe morphology in multicellular development, cultured cells were washed twice with DB- and resuspended at 1.0×10^7 cells/mL in DB + . A 10 μL cell suspension was placed on a 1.5% agar plate (Bacto-agar; dissolved in DB +), and excess liquid was allowed to evaporate. Each plate was incubated at 21 °C and observed at the indicated time points. Images were acquired with a camera (Moticam1000, SHIMADZU) attached to a stereo microscope (SZX10, Olympus) with a 1x objective lens (DE PLAPO 1X, Olympus).

Small population assay

Cells after a 4-h starvation were washed twice with DB- and resuspended at 3.0×10^6 cells/mL in DB + . At least 84 cell suspensions of 0.8 μL were plated on 1% agar plates (010-08725; Wako Pure Chemical Industries, Ltd.; dissolved in DB +), and excess liquid was allowed to evaporate. 0.8 μL DB+ containing cAMP (1 nM-1 μM) was plated next to the spots of the cell suspensions. The distance between the centers of a cell spot and a cAMP spot was kept at 2 mm. After incubation for 1 h, the fraction of cell spots in which the cells had accumulated on the high concentration side was measured.

Macropinocytosis assay

This experiment was performed as follows according to a previous report[99]. Cultured cells were resuspended at 5.0×10^6 cells/mL in fresh HL5 medium. A 2.5 mL cell suspension was transferred to a 20-mL Erlenmeyer flask and incubated for 15 min on a rotary shaker to allow the cells to recuperate. The assay was started by adding 50 μL TRITC-dextran solution (100 mg/mL TRITC-dextran 70, TdB Labs) to the cell suspension. At selected time points (0, 15, 30, 45, 60, 90, 120, 180 min), 250 μL aliquots were collected from the cell suspension on a rotary shaker and transferred to 2-mL tubes containing 25 μL Trypan Blue solution (2 mg/mL Trypan Blue, 20 mM citrate, 150 mM NaCl). The tubes were inverted once and centrifuged for 2 min at 800 × g. The supernatant was discarded, and the cells were washed once with 500 μL Soerensen buffer (2 mM Na_2HPO_4, 14.6 mM KH_2PO_4, pH 6.0) by centrifugation. The pellet was resuspended in 500 μL Soerensen buffer, and the fluorescence intensity was measured immediately with a fluorescence spectrophotometer (F2700, Hitachi-Hightech) (excitation 544 nm; emission 574 nm).

Phagocytosis assay

This experiment was performed as follows according to a previous report[99]. To label yeast with TRITC, 5 g of yeast (YSC-2, Sigma) was suspended in 50 mL PBS in a 100 mL Erlenmeyer flask and boiled at 100 °C for 30 min. The yeast suspension was centrifuged for 5 min at 3000 × g, and the supernatant was discarded. The yeast pellet was washed five times with 50 mL PBS and twice with 50 mL Soerensen buffer, and the density was adjusted to 2×10^{10} particles/mL with labeling buffer (50 mM Na_2HPO_4, pH 9.2) containing 0.1 mg/mL TRITC (87918, Sigma-Aldrich). After 30 min of incubation at 37 °C on a rotary shaker, 20 mL yeast suspension was washed twice with 20 mL labeling buffer and four times with 20 mL Soerensen buffer, and the density was adjusted to 1×10^9 particles/mL with Soerensen buffer. To quantify the phagocytosis rate, cultured cells were resuspended at 2.0×10^6 cells/mL in fresh HL5 medium. 5 mL of cell suspension was transferred to a 20-mL Erlenmeyer flask and incubated for 15 min on a rotary shaker to allow the cells to recuperate. The assay was started by adding 120 μL Soerensen buffer containing TRITC (87918, sigma)-labeled yeast to the cell suspension. At selected time points (0, 15, 30, 45, 60, 90, 120 min), 500 μL aliquots were collected from the cell suspension on a rotary shaker and transferred to 2-mL tubes containing 50 μL Trypan Blue solution. After 3 min of incubation, the cell suspension was centrifuged for 2 min at 800 × *g*, and the supernatant was discarded. The pellet was resuspended in 500 μL Soerensen buffer, and the fluorescence intensity was measured immediately with a fluorescence spectrophotometer (F2700, Hitachi-Hightech) (excitation 544 nm; emission 574 nm).

Kymographs of the fluorescence intensity on the cell membrane

The spatiotemporal dynamics of RBD_{Raf1}-RFP, mScarlet-I-RBD_{Raf1} and RasGEF-GFP in each cell were analyzed using a kymograph obtained as follows. The fluorescence intensity on the cell membrane was measured in space along the circumference of the cell divided into 90 sections of 4 degrees each and in time over 241 frames in the movie. This measurement yielded a two-dimensional matrix data for the i-th cell ($i = 1, 2, 3, \ldots N$) written as $mFI_i(s\Delta\theta, f\Delta t)$, where $s (s = 1, 2, 3, \ldots 90)$ and $f (f = 0, 1, 2, \ldots 240)$ denote the section and frame numbers with the intervals $\Delta\theta = 4$ degrees and $\Delta t = 5$ s. The data are displayed on the horizontal and vertical axes as a kymograph of 90 pixels × 241 pixels.

Quantification of domain size and period

The domain size was determined by binarizing the kymograph with the method of Li. The following process was performed to remove the influence of noise. In a binary image, each pixel was selected along with the immediately 5 adjacent left and right pixels (total of 11). If the majority of these pixels had a pixel value of 255, then the selected pixel was set to 255. Conversely, if the majority of these pixels had a pixel a

value of 0, then the selected pixel was set to 0. From the obtained binary images, the angle of the domain was calculated at each time point, and the angles were then averaged (Supplementary Fig. 3a). For the period, a temporal autocorrelation function of the fluorescence intensity at an arbitrary section of the cell circumference was calculated as,

$$tACF_i(s\Delta\theta,\tau\Delta t) = \frac{\sum_{f=0}^{240-\tau}\left(mFI_i(s\Delta\theta,f\Delta t)-\mu\right)\left(mFI_i(s\Delta\theta,(f+\tau)\Delta t)-\mu\right)}{(240-\tau)\varepsilon^2} \quad (1)$$

where μ and ε denote the mean and SD of the fluorescence intensity, respectively. $tACF_i$ was averaged over 90 sections, in which the lag-time, $\tau\Delta t$, giving the first peak was quantified as the period.

Classification of Ras-GTP dynamics into four patterns

The spatiotemporal dynamics of the activated form of Ras, Ras-GTP, in the excitable system showed four patterns: no generation of the Ras-GTP-enriched domain (no domain), transient generation of the domain (transient), traveling waves (wave) and uniform localization along the whole membrane (uniform), with increasing excitability in this order. Each cell consistently exhibited one of the four patterns during the 20-min observation. The spatiotemporal dynamics of Ras-GTP that spontaneously emerged in individual cells of each OE/KO strain was classified into the four patterns by hierarchical clustering[100]. The spatiotemporal dynamics in each cell was represented by a one-dimensional vector individually calculated from the kymograph as described below and subjected to hierarchical clustering using scipy 1.2.1. cluster.hierarchy. An iterative calculation was performed as follows. The initial condition of a single cell was represented by a component of the ensemble to be clustered, in which the centroid was calculated from the kymograph using the one-dimensional vector described below. The distance between two components was calculated for all possible pairs, and those with the nearest distance were combined as a new component, in which the centroid was calculated by averaging the two centroids. The calculation was repeated until all components were combined into one. The distance was calculated by Ward's method written as,

$$D_{jk} = \left(n_j \cdot \frac{n_k}{n_j+n_k}\right)\cdot\left|m_j-m_k\right|^2 \quad (2)$$

where $n_{j/k}$ and $m_{j/k}$ denote the number of combined components and the centroid of the j/k-th component, respectively. $|m_j-m_k|^2$ is the squared Euclidean distance between the centroids. Each pattern's clusters were determined based on the dendrogram by setting a threshold (Supplementary Fig. 2).

First, the cells were classified into two subgroups, those exhibiting a traveling wave and those exhibiting other patterns (Supplementary Fig. 2a, b). For this purpose, the following three quantitative expressions of the kymograph were exploited for the clustering to reveal periodicity in the dynamics: (1) The kymograph was normalized by the maximum fluorescence intensity around the cell periphery at each time point and smoothed with a Gaussian filter of $\sigma=1$, which is described as a vector, $\boldsymbol{K}_i^1=\left(mFI'_{isf}\right)_{1\le s\le 90,1\le f\le 241}$; (2) A temporal autocorrelation function for up to $t=120$ s, which is the duration when the periodicity is remarkable, was calculated from the kymograph smoothed with a Gaussian filter of $\sigma=5$, which was described as a vector, $\boldsymbol{K}_i^2=\left(tACF'_{is\tau}\right)_{1\le s\le 90,1\le\tau\le 121}$; and (3) A power spectrum was obtained by Fourier transforming $\boldsymbol{K}_i^2$ using

$$F(u,v)=\sum_{\tau=1}^{121}\sum_{s=1}^{90}\boldsymbol{K}_i^2(s,\tau)\exp\left(-2\pi i\left(\frac{us}{121}+\frac{v\tau}{90}\right)\right) \quad (3)$$

which was written as

$$P(u,v)=\left|F(u,v)\right|^2 \quad (4)$$

where (u,v) is the coordinates in the frequency domain. The maximum value, $Max(P(u,v))$, and its coordinates, $Max(u,v)$, of the power spectrum were described as a vector, $\boldsymbol{K}_i^3=(Max(P_{uv}),Max(u),Max(v))_{1\le s\le 90,1\le\tau\le 121}$. $\boldsymbol{K}_i^1$, $\boldsymbol{K}_i^2$ and $\boldsymbol{K}_i^3$ were combined and linearly transformed into a one-dimensional vector, which was subjected to hierarchical clustering.

The cells exhibiting other patterns were further classified into two subgroups, those exhibiting transient domains and those without domains (Supplementary Fig. 2c, d). For this purpose, the following two quantitative expressions of the kymograph were exploited for the clustering to reveal a spatial heterogeneity in the dynamics: (4) The kymograph was normalized as mentioned above as a vector, $\boldsymbol{K}_i^4=\left(mFI''_{isf}\right)_{1\le s\le 90,1\le f\le 241}$; and (5) A spatial autocorrelation function was calculated for up to $t=240$ s from the kymograph smoothed with a Gaussian filter of $\sigma=1$ as a vector, $\boldsymbol{K}_i^5=\left(spACF_{isf}\right)_{1\le s\le 90,1\le f\le 241}$, written as

$$sACF_i(s\Delta\theta,\tau\Delta t) = \frac{\sum_{s=0}^{89-\tau}\left(mFI_i(s\Delta\theta,f\Delta t)-\mu\right)\left(mFI_i((s+\varphi)\Delta\theta,f\Delta t)-\mu\right)}{(89-\tau)\varepsilon^2} \quad (5)$$

$\boldsymbol{K}_i^4$ and $\boldsymbol{K}_i^5$ were combined and linearly transformed into a one-dimensional matrix that was subjected to hierarchical clustering.

Next, the cells with other patterns were classified into two subgroups, those exhibiting a uniform domain and those exhibiting no domain (Supplementary Fig. 2e, f). For this purpose, the following quantitative expression of the kymograph was exploited for the clustering to reveal the fluorescence intensity on the plasma membrane. The fluorescence intensity of the plasma membrane was calculated by the spatio-temporal average of the kymograph: $\langle mFI_i(s\Delta\theta,f\Delta t)\rangle$; and the fluorescence intensity of the of the cytoplasm was calculated by the temporal average of the kymograph written as $\langle cFI_i(f\Delta t)\rangle$. The ratio of the fluorescence intensities at the plasma membrane and the cytoplasm was described as

$$\boldsymbol{K}_i^6=\frac{\langle mFI_i(s\Delta\theta,f\Delta t)\rangle}{\langle cFI_i(f\Delta t)\rangle} \quad (6)$$

and $\boldsymbol{K}_i^6$ was subjected to hierarchical clustering.

Classification of RasGEFs into clusters

The statistical distributions of the domain size and period of each RasGEF OE strain were displayed in a single heat map in domain size-period space (Supplementary Fig. 3). To obtain the heat map, we determined the domain size and period for each RasGEF OE strain as described above. We measured more than 100 cells for each RasGEF OE strain, from which we obtained the heat map with the domain size on the x-axis and period on the y-axis. The widths of the bins were determined based on Freedman-Diaconis' rule to be 30 s and 20 degrees assuming the cells showed traveling waves and domains, respectively. The data of all cells irrespective of the domain pattern were incorporated into the heat map by setting the summed probability density in each pattern equal to the fraction. Based on the extent of the excitability, the period of the cells exhibiting no domain (domain size = 0 degrees) was approximated as 460 s or the maximum value of the heat map, and that of the cells exhibiting uniform localization (domain size = 360 degrees) was approximated as 0 s or the minimum value. The period of cells exhibiting a transient domain of various sizes was approximated as 460 s. This approximation was

based on a previous simulation that showed the period becomes longer as the excitability decreases[28] and the fact that less than 1% of cells showing a traveling wave had a period of 450 s or longer. These heat maps were used for hierarchical clustering with Ward's method after linearly transforming them into one-dimensional vectors to classify RasGEFs based on the spatiotemporal characteristics of the Ras-GTP dynamics. Even if each RasGEF OE strain had the same fraction showing a travelling wave, this clustering method can analyze the similarities and differences between strains based on the different dynamics of Ras-GTP.

Subcellular localization analysis of RasGEFs

Time-lapse movies of RasGEF-GFP-expressing cells in the presence of latrunculin A acquired by confocal microscopy at 5-s intervals for 5 min were used for the analysis. After the effect of fluorescence photobleaching was corrected based on an approximation with an exponential function, a maximum projection of the movie stack was performed to obtain a still image to exclude artifacts of transient and localized reductions in the fluorescence intensity caused by intracellular vesicles that do not contain GFP. An image of the cell was elliptically approximated and divided into 10 regions by concentric ellipsoids at equal intervals: region 1 to region 10 from the inside to the outside of the cell (Supplementary Fig. 5). The fluorescence intensity was measured in the h-th region, FI_i^h, and all regions, FI_i^{all}, in the i-th cell. An index of localization to the h-th region, L_i^h, was written as.

$$L_i^h = \frac{FI_i^h}{FI_i^{all}} \tag{7}$$

L_i^h was averaged over N cells ($N \geq 7$). For uniform localization, the index approximates 1, and for membrane localization it is less than 1 in the inner regions and greater than 1 in the outer regions.

Co-localization analysis between RasGEFs and Ras-GTP

To examine the co-localization of RasGEFs and Ras-GTP, a cross-correlation function between the fluorescence intensity time series of GFP tagged to RasGEF and RFP or mScarlet-I tagged to RBD_{Raf1}, $mFI_i^{GEF}(s\Delta\theta, f\Delta t)$ and $mFI_i^{Ras}(s\Delta\theta, f\Delta t)$, respectively, simultaneously observed on the cell membrane in the i-th cell was calculated as

$$CCF_i(s\Delta\theta, \tau\Delta t) = \frac{\sum_{f=0}^{240}\left(mFI_i^{GEF}(s\Delta\theta, f\Delta t) - \mu_{GEF}\right)\left(mFI_i^{Ras}(s\Delta\theta, (f+\tau)\Delta t) - \mu_{Ras}\right)}{(240-\tau)\varepsilon_{GEF}\varepsilon_{Ras}} \tag{8}$$

where $\mu_{GEF/Ras}$ and $\varepsilon_{GEF/Ras}$ denote the mean and SD of the fluorescence intensities, respectively. CCF_i was averaged over 90 sections, and the coincidence between two traveling waves was confirmed.

Analysis of cytoskeleton-dependent protrusion dynamics

The frequency of the formation of pseudopods and macropinocytic cups and the size of the pseudopod were quantified in differential interference contrast images of RasGEF KO cells and laser confocal scanning microscopy images of RasGEF-GFP OE cells (Figs. 5 and 6). In this analysis, pseudopod (lamellipodia-like protrusions) and macropinocytic cup (macropinocytosis-associated protrusions) were distinguished. Pseudopods were defined as sustained membrane protrusions for at least 10 s, while macropinocytic cups were defined as cup-shaped concave structures. In an image of a cell at an arbitrary time, the pseudopodial region was determined as the region remaining after subtraction of an image of the same cell acquired 10 s before. If a pseudopod continued to extend in the same direction, it was considered a single pseudopod. If a pseudopod formed from a different region, it was considered a newly formed pseudopod. The number of newly formed pseudopods and macropinocytic cups over 5 min was counted, and the frequencies of the pseudopod formation and macropinocytic cup formation were calculated as the number per minute. Pseudopod size was calculated as the time average ratio in length of the perimeter section along the pseudopodial region to the entire perimeter of the cell preceding the image subtraction.

Cell migration analysis

The x- and y-coordinates of the centroid of the cell were obtained using laboratory-made software[5,6]. The migration trajectory was obtained at 5-s intervals ($\Delta t = 5$ s) for 30 min in spontaneous motility assays ($f\Delta t = 30$ min; $f = 1, \ldots, 360$) and 20 min in chemotaxis assays ($f\Delta t = 20$ min; $f = 1, \ldots, 240$). The migration speed, v_i, of the i-th cell ($i = 1, \ldots, N$) was quantified by averaging the instantaneous speed measured in a unit time window of $t'\Delta t = 120$ s over the trajectory as

$$v_i = \left\langle \left| \boldsymbol{p}_i((f+t')\Delta t) - \boldsymbol{p}_i(f\Delta t) \right| / \left(t'\Delta t/60\right) \right\rangle \tag{9}$$

where $\boldsymbol{p}_i(t)$ denotes the position at time t. The mean squared displacement (MSD) was defined as

$$MSD(f\Delta t) = \left\langle \left(\boldsymbol{p}_i((f+l)\Delta t) - \boldsymbol{p}_i(f\Delta t)\right)^2 \right\rangle_{l\Delta t, N} \tag{10}$$

where l is the frame number of the lag time. The chemotactic index, CI, of a cell, which indicates the efficiency of the chemotaxis, was quantified by averaging the cosine of the angle between two vectors, $\boldsymbol{p}_{t_r}$ and $\boldsymbol{p}_c$, which are the direction vectors from the start to the end position during an arbitrary 120 s and from the initial position, $\boldsymbol{p}_{initial}$, to the micropipette position, respectively, over the trajectory:

$$\mathrm{CI} = \langle \cos\theta \rangle = \left\langle \frac{\boldsymbol{p}_c \cdot \boldsymbol{p}_{t_r}}{|\boldsymbol{p}_c|\left|\boldsymbol{p}_{t_r}\right|} \right\rangle_r, \; r = 1, \ldots, 23 \tag{11}$$

cAMP response analysis

The fluorescence intensity of RBD_{Raf1}-RFP or mScarlet-I-RBD_{Raf1} was measured and averaged across the cell membrane, divided by the fluorescence intensity averaged in the cytoplasm, and normalized by the mean value before stimulating individual cells. A maximum intensity was detected in the time series after the moving average was taken and compared to a threshold value to evaluate the response of RBD_{Raf1}, which showed transient translocation to the cell membrane. Cells that exhibited a larger maximum intensity than the threshold were regarded as responsive, and a fraction of these cells was examined across the cAMP concentrations 1 pM to 10 μM. The concentration which induced a response in 50% of the cells (*i.e.*, EC_{50}) was estimated by fitting the dose-response plot to the equation

$$Y = A + \frac{B-A}{1+\left(\frac{X}{EC_{50}}\right)^C} \tag{12}$$

where A, B, c, X and Y denote the minimum value, the maximum value, Hill coefficient, cAMP concentration, and the fraction of responsive cells, respectively.

Quantification of cAMP oscillation period

In the time-lapse movies (800 pixels×600 pixels; 7.00 mm×5.25 mm) acquired every 30 s for 1 h starting around 4 h after the start of starvation, an image subtraction was performed for all neighboring frames, yielding a movie consisting of 120 frames showing frame-to-frame differences in brightness. A grid consisting of 81 squares, each

50 pixels×50 pixels (0.44 mm×0.44 mm) arranged in a 9 × 9 pattern, was overlaid onto the center of the movie. The brightness difference was summed in the square, and the time series was obtained for 81 squares. A temporal autocorrelation function of the brightness difference in the i-th square was calculated as

$$tACF_i(\tau\Delta t) = \frac{\sum_{f=0}^{120-\tau}\left(mFI_i(f\Delta t)-\mu\right)\left(mFI_i((f+\tau)\Delta t)-\mu\right)}{(120-\tau)\varepsilon^2} \quad (13)$$

where μ and ε denote the mean and SD of the brightness difference, respectively. $tACF_i$ was averaged over 81 squares, in which the lag-time, $\tau\Delta t$, giving the first peak was quantified as the period.

Reporting summary

Further information on research design is available in the Nature Portfolio Reporting Summary linked to this article.

Data availability

The datasets generated and analyzed in the current study are available in the Supplementary Information file and Source data. All other data that support the findings of this study are available from the corresponding authors upon request. Source data are provided with this paper.

Code availability

All Python and Image J scripts supporting the findings of this paper are available upon reasonable request.

References

1. Dennis Bray. *Cell Movements*. Garland Science. (1992).
2. Oosawa, F. Spontaneous signal generation in living cells. *Bull. Math. Biol.* **63**, 643–654 (2001).
3. Berg, H. C. E. *E. coli in Motion*. Springer-Verlag: New York, Inc. (2004).
4. Sasaki, A. T. et al. G protein-independent Ras/PI3K/F-actin circuit regulates basic cell motility. *J. Cell Biol.* **178**, 185–191 (2007).
5. Sato, M. J. et al. Input-output relationship in galvanotactic response of Dictyostelium cells. *BioSystems* **88**, 261–272 (2007).
6. Takagi, H., Sato, M. J., Yanagida, T. & Ueda, M. Functional analysis of spontaneous cell movement under different physiological conditions. *PLoS One* **3**, 1–7 (2008).
7. Parent, C. A. Making all the right moves: Chemotaxis in neutrophils and Dictyostelium. *Curr. Opin. Cell Biol.* **16**, 4–13 (2004).
8. Postma, M., Bosgraaf, L., Loovers, H. M. & Van Haastert, P. J. M. Chemotaxis: signalling modules join hands at front and tail. *EMBO Rep* **5**, 35–40 (2004).
9. Van Haastert, P. J. M. & Devreotes, P. N. Chemotaxis: signalling the way forward. *Nat. Rev. Mol. Cell Biol.* **5**, 626–634 (2004).
10. Janetopoulos, C. & Firtel, R. A. Directional sensing during chemotaxis. *FEBS Letters* **582**, 2075–2085 (2008).
11. Devreotes, P. N. et al. Excitable signal transduction networks in directed cell migration. *Annu. Rev. Cell Dev. Biol.* **33**, 103–125 (2017).
12. Matsuoka, S., Iwamoto, K., Shin, D. Y. & Ueda, M. Spontaneous signal generation by an excitable system for cell migration. *Front. Cell Dev. Biol.* **12**, 1–16 (2024).
13. Weiner, O. D., Marganski, W. A., Wu, L. F., Altschuler, S. J. & Kirschner, M. W. An actin-based wave generator organizes cell motility. *PLoS Biol* **5**, 2053–2063 (2007).
14. Arai, Y. et al. Self-organization of the phosphatidylinositol lipids signaling system for random cell migration. *Proc. Natl. Acad. Sci. USA.* **107**, 12399–12404 (2010).
15. Xiong, Y., Huang, C. H., Iglesias, P. A. & Devreotes, P. N. Cells navigate with a local-excitation, global-inhibition-biased excitable network. *Proc. Natl. Acad. Sci. USA.* **107**, 17079–17086 (2010).
16. Gerisch, G., Schroth-Diez, B., Müller-Taubenberger, A. & Ecke, M. PIP3 waves and PTEN dynamics in the emergence of cell polarity. *Biophys. J.* **103**, 1170–1178 (2012).
17. Yang, H. W., Collins, S. R. & Meyer, T. Locally excitable Cdc42 signals steer cells during chemotaxis. *Nat. Cell Biol.* **18**, 191–201 (2016).
18. Kortholt, A. & van Haastert, P. J. M. Highlighting the role of Ras and Rap during Dictyostelium chemotaxis. *Cell. Signal.* **20**, 1415–1422 (2008).
19. Swanson, J. A. Shaping cups into phagosomes and macropinosomes. *Nat. Rev. Mol. Cell Biol.* **9**, 639–649 (2008).
20. Clarke, M. et al. Curvature recognition and force generation in phagocytosis. *BMC Biol.* **8**, 154 (2010).
21. Veltman, D. M. et al. A plasma membrane template for macropinocytic cups. *Elife* **5**, 24 (2016).
22. Sasaki, A. T., Chun, C., Takeda, K. & Firtel, R. A. Localized Ras signaling at the leading edge regulates PI3K, cell polarity, and directional cell movement. *J. Cell Biol.* **167**, 505–518 (2004).
23. van Haastert, P. J. M., Keizer-Gunnink, I. & Kortholt, A. Coupled excitable Ras and F-actin activation mediates spontaneous pseudopod formation and directed cell movement. *Mol. Biol. Cell* **28**, 922–934 (2017).
24. Huang, C.-H., Tang, M., Shi, C., Iglesias, P. A. & Devreotes, P. N. An excitable signal integrator couples to an idling cytoskeletal oscillator to drive cell migration. *Nat. Cell Biol.* **15**, 1307–1316 (2013).
25. Miao, Y. et al. Altering the threshold of an excitable signal transduction network changes cell migratory modes. *Nat. Cell Biol.* **19**, 329–340 (2017).
26. Nishikawa, M., Hörning, M., Ueda, M. & Shibata, T. Excitable signal transduction induces both spontaneous and directional cell asymmetries in the phosphatidylinositol lipid signaling system for eukaryotic chemotaxis. *Biophys. J.* **106**, 723–734 (2014).
27. Tang, M. et al. Evolutionarily conserved coupling of adaptive and excitable networks mediates eukaryotic chemotaxis. *Nat. Commun.* **5**, 1–13 (2014).
28. Fukushima, S., Matsuoka, S. & Ueda, M. Excitable dynamics of Ras triggers spontaneous symmetry breaking of PIP3 signaling in motile cells. *J. Cell Sci.* **132**, jcs224121 (2019).
29. Banerjee, T. et al. Spatiotemporal dynamics of membrane surface charge regulates cell polarity and migration. *Nat. Cell Biol.* **24**, 1499–1515 (2022).
30. Biswas, D., Devreotes, P. N. & Iglesias, P. A. Three-dimensional stochastic simulation of chemoattractant-mediated excitability in cells. *PLoS Comput. Biol.* **17**, 1–29 (2021).
31. Shibata, T., Nishikawa, M., Matsuoka, S. & Ueda, M. Modeling the self-organized phosphatidylinositol lipid signaling system in chemotactic cells using quantitative image analysis. *J. Cell Sci.* **125**, 5138–5150 (2012).
32. Shibata, T., Nishikawa, M., Matsuoka, S. & Ueda, M. Intracellular encoding of spatiotemporal guidance cues in a self-organizing signaling system for chemotaxis in dictyostelium cells. *Biophys. J.* **105**, 2199–2209 (2013).
33. Kortholt, A. et al. Dictyostelium chemotaxis: essential Ras activation and accessory signalling pathways for amplification. *EMBO Rep* **12**, 1273–1279 (2011).
34. Kortholt, A., Keizer-Gunnink, I., Kataria, R. & Haastert, P. J. M. V. Ras activation and symmetry breaking during dictyostelium chemotaxis. *J. Cell Sci.* **126**, 4502–4513 (2013).
35. Veltman, D. M., Keizer-Gunnik, I. & Van Haastert, P. J. M. Four key signaling pathways mediating chemotaxis in Dictyostelium discoideum. *J. Cell Biol.* **180**, 747–753 (2008).
36. Tanabe, Y., Kamimura, Y. & Ueda, M. Parallel signaling pathways regulate excitable dynamics differently to mediate pseudopod

formation during eukaryotic chemotaxis. *J. Cell Sci.* **131**, jcs214775 (2018).
37. Artemenko, Y., Lampert, T. J. & Devreotes, P. N. Moving towards a paradigm: common mechanisms of chemotactic signaling in Dictyostelium and mammalian leukocytes. *CMLS* **71**, 3711–3747 (2014).
38. Wilkins, A. et al. The Dictyostelium genome encodes numerous RasGEFs with multiple biological roles. *Genome Biol* **6**, R68 (2005).
39. Insall, R. H., Borleis, J. & Devreotes, P. N. The aimless RasGEF is required for processing of chemotactic signals through G-protein-coupled receptors in Dictyostelium. *Curr. Biol.* **6**, 719–729 (1996).
40. Kortholt, A. et al. Characterization of the GbpD-activated Rap1 pathway regulating adhesion and cell polarity in Dictyostelium discoideum. *J. Biol. Chem.* **281**, 23367–23376 (2006).
41. Kae, H. et al. Cyclic AMP signalling in Dictyostelium: G-proteins activate separate Ras pathways using specific RasGEFs. *EMBO Rep* **8**, 477–482 (2007).
42. Mondal, S. et al. Linking Ras to myosin function: RasGEF Q, a Dictyostelium exchange factor for RasB, affects myosin II functions. *J. Cell Biol.* **181**, 747–760 (2008).
43. Charest, P. G. et al. A ras signaling complex controls the RasC-TORC2 pathway and directed cell migration. *Dev. Cell* **18**, 737–749 (2010).
44. Williams, T. D., Paschke, P. I. & Kay, R. R. Function of small GTPases in Dictyostelium macropinocytosis. *Philos. Trans. R. Soc. B Biol. Sci.* **374**, 20180150 (2019).
45. Lin, X. P., Mintern, J. D. & Gleeson, P. A. Macropinocytosis in different cell types: Similarities and differences. *Membranes (Basel)* **10**, 1–21 (2020).
46. Swanson, J. A. & King, J. S. The breadth of macropinocytosis research. *Philos. Trans. R. Soc. B Biol. Sci.* **374**, 20180146 (2019).
47. Commisso, C. et al. Macropinocytosis of protein is an amino acid supply route in Ras-transformed cells. *Nature* **497**, 633–637 (2013).
48. Ramirez, C., Hauser, A. D., Vucic, E. A. & Bar-Sagi, D. Plasma membrane V-ATPase controls oncogenic RAS-induced macropinocytosis. *Nature* **576**, 477–481 (2019).
49. Bloomfield, G. & Kay, R. R. Uses and abuses of macropinocytosis. *J. Cell Sci.* **129**, 2697–2705 (2016).
50. Hoeller, O. et al. Two distinct functions for PI3-kinases in macropinocytosis. *J. Cell Sci.* **126**, 4296–4307 (2013).
51. Bloomfield, G. et al. Neurofibromin controls macropinocytosis and phagocytosis in Dictyostelium. *Elife* **2015**, 1–25 (2015).
52. Marinovic, M. et al. IQGAP-related protein IqgC suppresses Ras signaling during large-scale endocytosis. *Proc. Natl. Acad. Sci. USA.* **116**, 1289–1298 (2019).
53. Killich, T. et al. The locomotion, shape and pseudopodial dynamics of unstimulated Dictyostelium cells are not random. *J. Cell Sci.* **106**, 1005–1013 (1993).
54. Hacker, U., Albrecht, R. & Maniak, M. Fluid-phase uptake by macropinocytosis in dictyostelium. *J. Cell Sci.* **110**, 105–112 (1997).
55. Bosgraaf, L. & Van Haastert, P. J. M. The ordered extension of pseudopodia by amoeboid cells in the absence of external cues. *PLoS One* **4**, e5253 (2009).
56. Insall, R. H. Understanding eukaryotic chemotaxis: A pseudopod-centred view. *Nat. Rev. Mol. Cell Biol.* **11**, 453–458 (2010).
57. Gerisch, G., Ecke, M., Wischnewski, D. & Schroth-Diez, B. Different modes of state transitions determine pattern in the Phosphatidylinositide-Actin system. *BMC Cell Biol.* **12**, 42 (2011).
58. Lutton, J. E. et al. Formation and closure of macropinocytic cups in Dictyostelium. *Curr. Biol.* **33**, 3083–3096.e6 (2023).
59. Sasaki, A. T. & Firtel, R. A. Regulation of chemotaxis by the orchestrated activation of Ras, PI3K, and TOR. *Eur. J. Cell Biol.* **85**, 873–895 (2006).
60. Lim, C. J., Spiegelman, G. B. & Weeks, G. Cytoskeletal regulation by Dictyostelium Ras subfamily proteins. *J. Muscle Res. Cell Motil.* **23**, 729–736 (2002).
61. Kae, H., Lim, C. J., Spiegelman, G. B. & Weeks, G. Chemoattractant-induced Ras activation during Dictyostelium aggregation. *EMBO Rep* **5**, 602–606 (2004).
62. Maeda, Y. T., Inose, J., Matsuo, M. Y., Iwaya, S. & Sano, M. Ordered patterns of cell shape and orientational correlation during spontaneous cell migration. *PLoS One* **3**, e3734 (2008).
63. Parikh, A. et al. Conserved developmental transcriptomes in evolutionarily divergent species. *Genome Biol* **11**, R35 (2010).
64. Nichols, J. M. E. et al. The atypical MAP Kinase ErkB transmits distinct chemotactic signals through a core signaling module. *Dev. Cell* **48**, 491–505.e9 (2019).
65. Bindels, D. S. et al. MScarlet: A bright monomeric red fluorescent protein for cellular imaging. *Nat. Methods* **14**, 53–56 (2016).
66. Bosgraaf, L. et al. RasGEF-containing proteins GbpC and GbpD have differential effects on cell polarity and chemotaxis in Dictyostelium. *J. Cell Sci.* **118**, 1899–1910 (2005).
67. Kamimura, Y., Miyanaga, Y. & Ueda, M. Heterotrimeric G-protein shuttling via Gip1 extends the dynamic range of eukaryotic chemotaxis. *Proc. Natl. Acad. Sci. USA.* **113**, 4356–4361 (2016).
68. Kamimura, Y. & Ueda, M. Different heterotrimeric g protein dynamics for wide-range chemotaxis in eukaryotic cells. *Front. Cell Dev. Biol.* **9**, 1–8 (2021).
69. Iglesias, P. A. & Devreotes, P. N. Biased excitable networks: How cells direct motion in response to gradients. *Curr. Opin. Cell Biol.* **24**, 245–253 (2012).
70. Edwards, M. et al. Insight from the maximal activation of the signal transduction excitable network in Dictyostelium discoideum. *Proc. Natl. Acad. Sci. USA.* **115**, E3722–E3730 (2018).
71. Arigoni, M. et al. A novel Dictyostelium RasGEF required for chemotaxis and development. *BMC Cell Biol* **6**, 1–18 (2005).
72. Eldar, A. & Elowitz, M. B. Functional roles for noise in genetic circuits. *Nature* **467**, 167–173 (2010).
73. Norman, T. M., Lord, N. D., Paulsson, J. & Losick, R. Stochastic switching of cell fate in microbes. *Annu. Rev. Microbiol.* **69**, 381–403 (2015).
74. Meron, E. Pattern formation in excitable media. *Phys. Rep.* **218**, 1–66 (1992).
75. Lindner, B., García-Ojalvo, J., Neiman, A. & Schimansky-Geier, L. Effects of noise in excitable systems. *Phys. Rep.* **392**, 321–424 (2004).
76. Bonfini, L., Karlovich, C. A., Dasgupta, C. & Banerjee, U. The son of sevenless gene product: a putative activator of ras. *Science* **255**, 603–606 (1992).
77. Baltanás, F. C., Zarich, N., Rojas-Cabañeros, J. M. & Santos, E. SOS GEFs in health and disease. *Biochim. Biophys. Acta - Rev. Cancer* **1874**, 188445 (2020).
78. Boriack-Sjodin, P. A., Margarit, S. M., Bar-Sagi, D. & Kuriyan, J. The structural basis of the activation of Ras by Sos. *Nature* **394**, 337–343 (1998).
79. Boykevisch, S. et al. Regulation of ras signaling dynamics by sos-mediated positive feedback. *Curr. Biol.* **16**, 2173–2179 (2006).
80. Cherfils, J. & Zeghouf, M. Regulation of small GTPases by GEFs, GAPs, and GDIs. *Physiol. Rev.* **93**, 269–309 (2013).
81. Nakamura, Y., Umeki, N., Abe, M. & Sako, Y. Mutation-Specific Mechanisms of Hyperactivation of Noonan Syndrome SOS Molecules Detected with Single-molecule Imaging in Living Cells. *Sci. Rep.* **7**, 1–10 (2017).
82. King, J. S. & Kay, R. R. The origins and evolution of macropinocytosis. *Philos. Trans. R. Soc. B Biol. Sci.* **374**, 1765 (2019).
83. Salloum, G., Bresnick, A. R. & Backer, J. M. Macropinocytosis: Mechanisms and regulation. *Biochem. J.* **480**, 335–362 (2023).

84. Bolourani, P., Spiegelman, G. B. & Weeks, G. Delineation of the roles played by rasg and rasc in camp-dependent signal transduction during the early development of dictyostelium discoideum. **17**, 4543–4550 (2006).
85. Bruckert, F. et al. Dictyostelium discoideum adhesion and motility under shear flow: Experimental and theoretical approaches. *J. Muscle Res. Cell Motil.* **23**, 651–658 (2002).
86. Décavé, E. et al. Shear flow-induced motility of Dictyostelium discoideum cells on solid substrate. *J. Cell Sci.* **116**, 4331–4343 (2003).
87. Sato, M. J. et al. Switching direction in electric-signal-induced cell migration by cyclic guanosine monophosphate and phosphatidylinositol signaling. *Proc. Natl. Acad. Sci. USA.* **106**, 6667–6672 (2009).
88. Van Duijn, B. & Inouye, K. Regulation of movement speed by intracellular pH during Dictyostelium discoideum chemotaxis. *Proc. Natl. Acad. Sci. USA.* **88**, 4951–4955 (1991).
89. Nishimura, S. I., Ueda, M. & Sasai, M. Cortical factor feedback model for cellular locomotion and cytofission. *PLoS Comput. Biol.* **5**, e1000310 (2009).
90. Nishimura, S. I., Ueda, M. & Sasai, M. Non-Brownian dynamics and strategy of amoeboid cell locomotion. *Phys. Rev. E - Stat. Nonlinear, Soft Matter Phys* **85**, 1–8 (2012).
91. Beta, C., Edelstein-Keshet, L., Gov, N. & Yochelis, A. From actin waves to mechanism and back: How theory aids biological understanding. *Elife* **12**, 1–37 (2023).
92. Bement, W. M., Goryachev, A. B., Miller, A. L. & von Dassow, G. Patterning of the cell cortex by Rho GTPases. *Nat. Rev. Mol. Cell Biol.* **25**, 290–308 (2024).
93. Watts, D. J. & Ashworth, J. M. Growth of myxameobae of the cellular slime mould Dictyostelium discoideum in axenic culture. *Biochem. J.* **119**, 171–174 (1970).
94. Fujimoto, K., Nakano, K., Kuwayama, H. & Yumura, S. Deletion of gmfA induces keratocyte-like migration in Dictyostelium. *FEBS Open Bio* **12**, 306–319 (2022).
95. Sekine, R., Kawata, T. & Muramoto, T. CRISPR/Cas9 mediated targeting of multiple genes in Dictyostelium. *Sci. Rep.* **8**, 1–11 (2018).
96. Engler, C., Kandzia, R. & Marillonnet, S. A one pot, one step, precision cloning method with high throughput capability. *PLoS One* **3**, e3647 (2008).
97. Kuwayama, H. et al. PCR-mediated generation of a gene disruption construct without the use of DNA ligase and plasmid vectors. *Nucleic Acids Res* **30**, 2–6 (2002).
98. Jeon, T. J., Lee, D. J., Merlot, S., Weeks, G. & Firtel, R. A. Rap1 controls cell adhesion and cell motility through the regulation of myosin II. *J. Cell Biol.* **176**, 1021–1033 (2007).
99. Rivero, F. & Maniak, M. Quantitative and microscopic methods for studying the endocytic pathway. *Methods Mol. Biol.* **346**, 423–438 (2006).
100. Joe, H. & Ward, J. Hierarchical grouping to optimize an objective function. *J. Am. Stat. Assoc.* **58**, 236–244 (1963).

Acknowledgements

We thank Dr. Peter Karagiannis for critical reading of the manuscript and Dr. Satoshi Sawai and Dr. Hidenori Hashimura for mScarlet-I-RBD$_{Raf1}$ (pDM1208_mScarlet-I-hRaf1RBD_coaA:HygR). We also thank NBRP for the tremendous support. This work was supported by funds from the Japan Society for the Promotion of Science (JSPS) Grant-in-Aid for JSPS Research Fellow grant no. 22KJ2207 to KI, JSPS KAKENHI grants no. 19H00982 to MU and no. 19H05798 to SM, Japan Science and Technology Agency grant no. JPMJPR1879 to SM and JPMJCR21E1 to MU, and Japan Agency for Medical Research and Development grant no. JP20gm0910001 to MU.

Author contributions

Conceptualization, K.I., S.M., and M.U.; Methodology, K.I., S.M., and M.U.; Software, K.I.; Validation, K.I., S.M., and M.U.; Formal analysis, K.I.; Investigation, K.I.; Resources, K.I., S.M., and M.U.; Data curation, K.I.; Writing - original draft, K.I.; Writing - review &editing, K.I., S.M., and M.U.; Visualization, K.I.; Supervision, M.U.; Project administration, S.M. and M.U.; Funding acquisition, K.I., S.M., and M.U.

Competing interests

The authors declare no competing interests.

Additional information

Supplementary information The online version contains supplementary material available at https://doi.org/10.1038/s41467-024-55389-2.

Correspondence and requests for materials should be addressed to Satomi Matsuoka or Masahiro Ueda.

Peer review information *Nature Communications* thanks Arjan Kortholt and the other, anonymous, reviewer(s) for their contribution to the peer review of this work. A peer review file is available.